Contributions of precision engineering to the revision of the SI

Contents lists available at SciVerse ScienceDirect

CIRP Annals Manufacturing Technology

Journal homepage: www.elsevier.com/locate/cirp

Contributions of precision engineering to the revision of the SI

Harald Bosse (3)[a,*], Horst Kunzmann (1)[a], John Pratt (3)[b], Stephan Schlamminger(3)[b], Ian Robinson (3)[c], Michael de Podesta (3)[c], Paul Shore (3)[c], Alessandro Balsamo (1)[d], Paul Morantz [e]

[a] *Physikalisch-Technische Bundesanstalt (PTB), Braunschweig, Germany*
[b] *National Institute of Standards and Technology (NIST), Gaithersburg, MD, USA*
[c] *National Physical Laboratory (NPL), Teddington, United Kingdom*
[d] *Istituto Nazionale di Ricerca Metrologica (INRIM), Torino, Italy*
[e] *Cranfield University, Cranfield, United Kingdom*

All measurements performed in science and industry are based on the International System of Units, the SI. It has been proposed to revise the SI following an approach which was implemented for the redefinition of the unit of length, the metre, namely to define the SI units by fixing the numerical values of so-called defining constants, including *c*, *h*, *e*, *k* and N_A. We will discuss the reasoning behind the revision, which will likely be put into force in 2018. Precision engineering was crucial to achieve the required small measurement uncertainties and agreement of measurement results for the defining constants.

Keywords: Metrology, System, Revised SI

1. Introduction

"*In physical science the first essential step in the direction of learning any subject is to find principles of numerical reckoning and practicable methods for measuring some quality connected with it*" [182]. This statement of Lord Kelvin stresses the importance of measurement for an increase of knowledge in science, but is also valid in a broader sense. Measurements have always been regarded as necessary information for advancement of science, manufacturing, trade and daily life since the ancient times. Moreover, to assure the reliability of measurements, the development and maintenance of a suitable system of units, to which the measurement results have to be referred, have always been considered as governmental responsibility.

The concept of interchangeable parts allows to manufacture a component and provides confidence that it will fit with other components manufactured many years earlier in a different part of the world without the need for adjustment. What is remarkable about this is that it is no longer remarkable, but in fact completely expected. This is due to our measurement and quality assurance systems that enable traceability of measurement results to the base units of the International System of Units, the SI. The SI is a metric system published in 1960 by the General Conference for Weights and Measures (CGPM) [20] and it is the internationally recommended and most widely used system of units.

An example of an incorrect use of different systems of units is known from the National Aeronautics and Space Administration (NASA) spacecraft mission *Mars Climate Orbiter*. The spacecraft was lost in 1999 because momentum control output was specified in non-SI units of pound-seconds (lbf s) instead of the SI units of newton-seconds (N s) [173].

Historically, definitions of units have changed over time following the progress of science. For example, definition of the unit of length changed from artefact-based definitions (i.e. metre bar) to the wavelength-based definition in 1960. The current definition of the length unit, adopted in 1983, is a time of flight definition and is based on fixing the numerical value of the speed of light in vacuum, *c*. A system of units has to be not only reliable and consistent but also flexible enough to support further progress of science.

At the heart of the present SI are definitions of seven 'base units', namely the metre with the unit symbol (m) for the quantity of length, the kilogram (kg) for the mass, the second (s) for the time, the ampere (A) for the electric current, the kelvin (K) for the thermodynamic temperature, the mole (mol) for the amount of substance and the candela (cd) for the luminous intensity. In addition, so-called derived units in the SI are formed by powers, products or quotients of the base units to describe other quantities.

Uncertainty in the definitions of the base units represent insurmountable obstacles to the progress of metrology and science. It is not possible to make SI measurements more accurately than the measurement units can be realised. With this in mind, the General Conference of Weights and Measures (CGPM) has encouraged the metrology community *to complete all work necessary for the CGPM at its 26th meeting* (in 2018) *to adopt a resolution that would replace the current SI with the revised SI, provided the amount of data, their uncertainties, and level of consistency are deemed satisfactory* [36].

The principle of the revised SI is to fix the numerical values of seven so-called defining constants rather than relying on a specific material property (as in the case of the kelvin today), or a specific artefact (as currently in the case of the kilogram). This principle was implemented in 1967 for the unit of the time, the second, and based on this definition for the unit of length: in 1983 the metre was defined by fixing the numerical value of a fundamental constant, the speed of light in vacuum, *c* to $c = 299\,792\,458$ m/s.

This approach is proposed to be followed for the redefinition of all units and in particular of four base units: In addition to the numerical value of the transition between the two hyperfine levels of the ground state of the caesium 133 atom $\Delta\nu_{Cs}$ and the one of the speed of light *c*, those of the Planck constant *h*, the

Boltzmann constant k, the elementary charge e and the Avogadro constant N_A will be fixed as well.

The adoption of these definitions means that the practical realisation of any unit and in particular the base units can be undertaken using the equations of physics along with any appropriate technology. Thus, as technology advances over the coming centuries – in ways that we cannot foresee – these definitions of base units can still be used. In contrast, the artefact-based definitions bound to change over time (see Fig. 11). For example, the International Prototype of the kilogram (IPK) does not weigh one kilogram until it has been cleaned by rubbing with a goatskin – a chamois leather. Such arcane practices may be acceptable for the realisation of a unit, but should no longer be part of its definition.

The consistency of the current SI system with the proposed revised SI requires high precision measurements of the newly proposed defining constants, namely h, k, e and N_A using different measurement methods. It will be shown in this paper that precision manufacturing and precision engineering plays a vital role to pave the way to the revised SI.

2. Historical evolution of the system of units

A system of units as a base for measurements is necessary for all developed countries, starting with ancient civilizations. As an example it is known from ancient Egypt that a system of weights and measures was developed, whose standards were maintained by civil servants of the Pharaoh. The base unit of length was the Egyptian royal cubit (forearm), a standard of about 52.3 cm length (7 palms) made of either stone or (gold covered) wood with divisions showing smaller length units (palms, fingers), see Fig. 1 [104, 168].

Fig. 1. Copy of an Egyptian cubit.

Wooden copies of the royal cubit were used for length measurements in daily life (Fig. 2). Famous examples of the achieved accuracy in construction tasks in ancient Egypt are the pyramids. For example, the Cheops pyramid, built 2500 years BC shows the following small length and angle deviations: < 4 cm side length deviation over 230 m; < 1′ deviation from 90° at base (7 cm/230 m); < 2.8′ deviation from north-south direction; < 2 cm deviation from horizontal plane at the base [24].

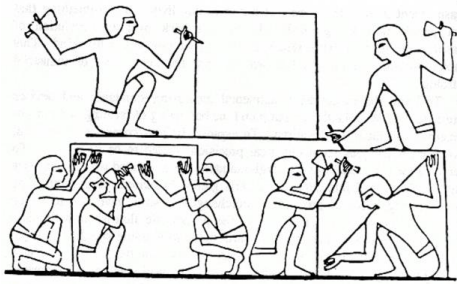

Fig. 2. One of the earliest records of geometrical measurement: Egyptian wall painting in the tomb of Rekh-mi-re' at Thebes built 1440 BC [46].

An example of a length measurement instrument from another ancient culture is shown in Fig. 3.

Fig. 3. Vernier caliper (9 AC) from Chinese Han dynasty [76].

Until the end of the 18th century the different length standards were based on graduated scales, usually deduced from body dimensions (inch (FR: pouce, DE: Zoll), cubit (aune, Elle), foot (pied, Fuß), fathom (toise, Klafter) of leading persons of the political systems (pharaoh, emperor, king, sovereign). However, some examples were reported which also used different approaches, as the definition of a mean foot illustrated in Fig. 4.

In the pre-industrialised era, the large variety of different national, regional or local length standards resulted in barriers to trade because producers and merchants had to show that they complied with the local length standards when selling their goods. Usually, the local standard or a copy of it was mounted close to the market place for direct reference, Fig. 5 shows one example.

Driven by the requirements from early industrialisation and associated concepts like the interchangeability of parts at the end of the 18th century, the need for a more precise and robust length standard was identified, which ideally should also be widely adopted in the industrialised nations.

Fig. 4. Definition of a mean foot as length unit [97].

Fig. 5. 'Braunschweiger Elle', the local length standard mounted close to the Old Town Market of the city of Braunschweig, Germany [courtesy PTB].

In France it was decided to avoid relating the length unit to human dimensions, but to refer it to a natural stable reference: the length of the earth meridian. The required triangulation measurements passing the cities of Dunkerque, Paris and Barcelona were finished by Delambre and Méchain in 1795 [1], see Fig. 6. The 1/10 000 000 part of the quarter meridian, so measured, was defined as a new length unit: the metre.

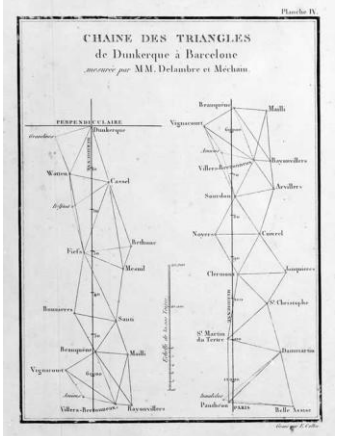

Fig. 6. Part of triangulation map between Dunkerque and Barcelona used for the definition of the Mètre des Archives [47].

In 1799, a platinum bar, the 'Mètre des Archives' was defined as the first metric length standard, see Fig. 7.

Fig. 7. Mètre des Archives [95].

The metric system was internationally accepted on the 20th of May, 1875 by 17 national states, the first signatories of the so-called *Metre Convention*. The International Bureau of Weights and Measures (BIPM) in Sèvres also was founded in this year to foster international acceptance of the metric system as a base for development of science, industry and international trade [155]. Soon after the work of the BIPM started, also national metrology institutes (NMI's) were established to disseminate the metric units in their countries and to perform research in metrology, the 'science of measurement and its application' (Physikalisch-Technische Reichsanstalt (PTR) in Germany in 1887, National Physical Laboratory (NPL) in the United Kingdom in 1900, and National Bureau of Standards (NBS) in the United States of America in 1901).

At the first General Conference of Weights and Measures (CGPM) in 1889 the length of the international metre prototype (Pt-Ir alloy (90% platinum, 10% iridium) produced by Johnson Matthey in London, x-shaped cross-section), or to be more precise the distance of its line engravings at ice water temperature was defined as the length unit traceable to the former 'Mètre des Archives'. High precision length measurements could be performed at relative uncertainty (u_r) levels of 10^{-7} by making use of national metre prototypes maintained at the NMI's (Fig. 8), which were compared to the international metre prototype.

Fig. 8. Copy #23 of international metre prototype [courtesy PTB].

Around the time the first CGPM took place, first interferometric measurements were already performed by Michelson and Morley. It took, however, until 1960 until the scale based definition of the length unit was replaced by a wavelength based definition at the 11th CGPM. It was decided to use the orange line of the krypton-86 isotope ($\lambda \approx 606$ nm) as the new vacuum wavelength standard, based on intensive investigations of stable gas discharge light sources with long coherence length which allowed improvements in interferometric precision [8]. Based on this definition high precision length measurements with relative uncertainties of about 10^{-8} could be performed. In 1960 also the laser was invented, which then offered new possibilities in interferometry.

In 1983 it was decided to change the definition of the length unit once again, because the uncertainty for measurement of the speed of light approached the accuracy for realization of the length unit [57], see Fig. 9. It was thus decided to fix the best known value of the speed of light in vacuum (c = 299 792 458 m/s) and to use this value of c for definition of the length unit:

The metre is the length of the path travelled by light in vacuum during a time interval of 1/ 299 792 458 of a second.

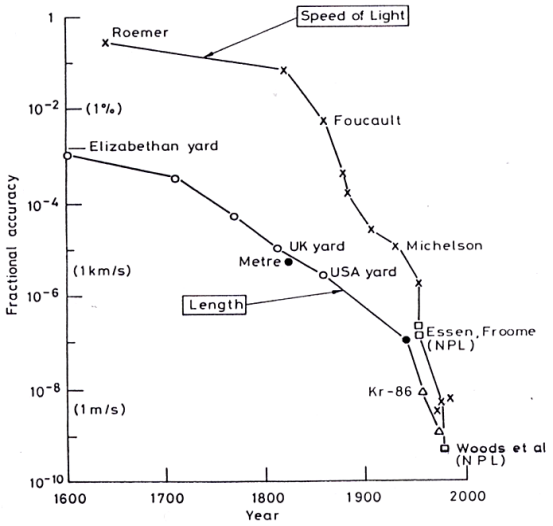

Fig. 9. Improvements in the accuracy of realisation of the unit of length and measurement of the speed of light [141].

As already noted, the approach to fix the best-known value of a natural constant and to then define a unit by this numerical value also serves as a blueprint for the discussed redefinition of the SI-system [22].

The time of flight definition of the length unit can directly be used for long range measurements, like e.g. lunar laser ranging [140] or long distance metrology in geodesy [147] and large scale manufacturing [167]. For applications in normal laboratory and manufacturing environment, since time-of-flight measurements do not provide the necessary accuracy over smaller lengths, interferometric length measurements based on recommended stabilized light sources offer smallest uncertainties. For precision length interferometry the recommended stabilized light sources and their operation conditions are described in the Mise en pratique [21]. Well known examples are the iodine-stabilized red HeNe laser at $\lambda \approx 633$ nm offering a relative uncertainty of the vacuum wavelength of 2.1×10^{-11} or the iodine-stabilized frequency-doubled green Nd:YAG laser at $\lambda \approx 532$ nm offering a relative uncertainty of the vacuum wavelength of 8.9×10^{-12}. The unstabilized HeNe laser at $\lambda \approx 633$ nm could also be used for interferometric length measurements if its relative uncertainty of 1.5×10^{-6} is sufficient for the given application, as e.g. the shape measurement of precision flats by interferometry.

Information on the use of the current SI can be found e.g. in [180]. The economic impact of measurement systems in general was addressed in different studies, an example for the UK is given in [99].

3. Background and proposal for the revised SI

3.1 The current SI and its limitations

The reasoning behind the proposed redefinition of the SI has been addressed in several publications, see e.g. [123]. The main reason is that in the current SI system the definition of the kilogram is still directly artefact based. The kilogram is defined by the mass of the International Prototype of the Kilogram (IPK), a Pt-Ir cylinder with 39 mm height and diameter, which is maintained at the BIPM in Sèvres since 1889 [45], see Fig. 10.

The IPK has been in use in comparison measurements with its 6 official copies at the BIPM (témoins) and the other copies

maintained at the NMI's only 3 times since the first comparisons in 1889.

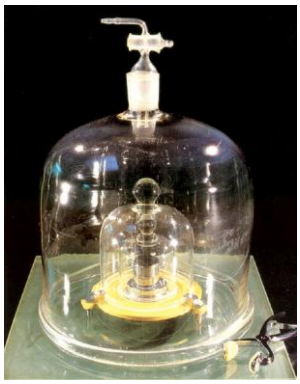

Fig. 10. International kilogram prototype [courtesy BIPM].

The results of the performed re-calibrations over the years indicate a tendency of an increase of mass of the kilogram copies in the order of about 50 µg or to put it the other way round a possible decrease of the mass of the IPK, see Fig. 11 [175].

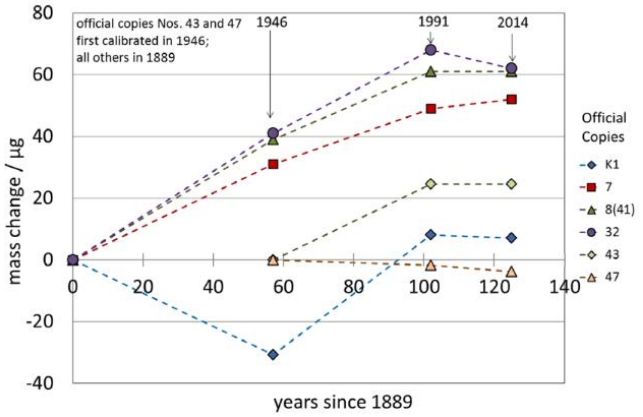

Fig. 11. Results of calibrations of the official IPK copies at BIPM to the IPK over the years. [175]

Possible reasons for the observed long-term instability of the IPK e.g. diffusion effects in the Pt-Ir alloy material or influences of the cleaning procedures [86, 110] of the mass prototypes were discussed in literature but an unambiguous reason could not be identified. As a result of the recent loop of Extraordinary Calibrations at the BIPM corrections of the masses of national prototypes were recommended [31].

The observed level of instability of about 50 µg ($5 \cdot 10^{-8}$) has to be compared with the current level of measurement uncertainty for 1 kg mass standards in air offered by NMI's. Examples of expanded measurement uncertainties U ($k = 2$), specified as calibration and measurement capabilities (CMC) in the BIPM key comparison data base (KCDB) [90] are: 28 µg (DE, IT, KO), 30 µg (AU, CD, FR, UK), 32 µg (US), 40 µg (CD), 50 µg (CH, RU) and 58 µg (JP).

Per definition, the uncertainty of the mass of the IPK is zero, however its observed instability is in the order of specified measurement uncertainties for high precision mass calibrations of NMIs. Moreover, for the dissemination of the mass unit accredited calibration laboratories or verification authorities are important, which have specified calibration uncertainties down to 80 µg for the highest quality grade mass standards (grade E1).

Another example of a definition of a SI-unit which is dependent on material properties is the definition of the temperature scale. The kelvin, unit of thermodynamic temperature, is currently defined as *"the fraction 1/273.16 of the thermodynamic temperature of the triple point of water"*. The triple point generally is defined as the temperature in which all three phases (gas, liquid, and solid) of a substance coexist in thermodynamic equilibrium (Fig. 12). It is known that the triple point temperature depends on the purity and isotopic composition of water. Therefore, a specific type of water has to be chosen as reference (see chapter 5).

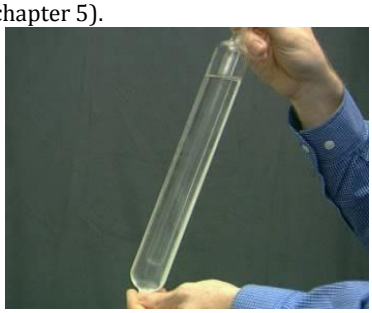

Fig. 12. A triple point cell of water [courtesy PTB].

Another concern with the current SI system of units is that high precision electrical measurements are no longer fully integrated in the SI system. The current definition of the ampere reads:

The ampere is that constant current which, if maintained in two straight parallel conductors of infinite length, of negligible circular cross-section, and placed 1 m apart in vacuum, would produce between these conductors a force equal to 2 x 10^{-7} newton per metre of length.

Please note that this definition also defines the permeability of vacuum or magnetic constant μ_0 to be exactly $\mu_0 = 4\ \pi \times 10^{-7}$ and that it is an idealisation assuming both, infinite and negligible dimensions. The accuracy of *direct* practical realizations of the ampere in the current SI by so-called current balances have been shown to be restricted to a few parts in 10^6 [186].

In practice high precision electrical measurements today rely on the application of electrical quantum standards and their associated superior reproducibility for the derived units of voltage and resistance. Josephson standards allow the realization of voltages in quantized steps of $U_J = h \cdot f/2e$, with h being Planck's constant, e the elementary charge and f the frequency of the microwaves driving the Josephson junction [87]. The well-defined resistance plateaus of $R_K = h/e^2$ provide a quantised resistance standard accurately related to fundamental constants [187]. In 1988 the International Committee for Weights and Measures (CIPM) adopted two recommendations which set exact values for the Josephson constant $K_{J\text{-}90} = 44597.9$ GHz/V ($K_J = 2e/h$) and the von Klitzing constant $R_{K\text{-}90} = 25\,812.807\ \Omega$ and called for laboratories to base their standards on these 'conventional' values from January 1st, 1990 [154]. This reference to quantum standards allowed electrical measurements, based on these units, to be made at a reproducibility level of about 10^{-9}.

3.2. The proposed revision of the SI

The proposal to define a system of units on atomic and molecular properties was already proposed by Maxwell in 1870 [113]: *If we wish to obtain standards of length, time and mass, which will be absolutely permanent, we must seek them not in the dimension or the motion or the mass of our planet but in the wavelength, the period of vibration and the absolute mass of these imperishable and unalterable and perfectly similar molecules.*

Planck proposed a definition of a system of units based on natural constants in 1900 [144]. He argued to use as defining constants the speed of light in vacuum c, the Boltzmann constant k, the gravitational constant G and a constant h, which later on was called Planck's constant, which he introduced in 1900 to describe quantised energy transfer. Based on this assumption, which is regarded as the birth of quantum theory, he was able to consistently describe precise measurement results of the spectral intensity of black body radiation which was not possible using

theories existing at the time [145]. With the exception of G, which is known today with a relative standard uncertainty of only 4.7 x 10^{-5}, the other natural constants proposed by Planck are known with better precision and thus were proposed to be used in the revised SI.

The approach taken in 1983 for the new definition of the metre, namely to define the unit of length, the metre, by fixing the numerical value of the speed of light in vacuum thus already followed Planck's proposal and also served as a model for the revised SI. This approach also moves away from the dependence on material artefacts and material properties and opens new options for different concepts of realisation and dissemination of the units as will be discussed later in this paper.

As mentioned before, the defining constants of the revised SI are proposed to be: $\Delta\nu$, c, h, e, k, N_A, $K_{CD.}$ Using those and experiments based on the equation of physics, the units can be realized. For example, measuring the frequency of the hyperfine transition in the caesium 133 atom provides the second. The measured length, light proceeds in one second at the speed of light in vacuum realizes the metre. The ampere might be realized by counting the number of electrons passing through an electric circuit within one second. However, by just counting electrons, the coulomb might be realized directly or the resistance by determining the von Klitzing constant in a superconducting two-dimensional conductor. The latter two examples show, that there is nothing special any more about the former "base" units even though they are maintained for convenience. As these examples show, in most cases more than one defining constant is needed to realize a unit (Fig. 13, Fig. 14).

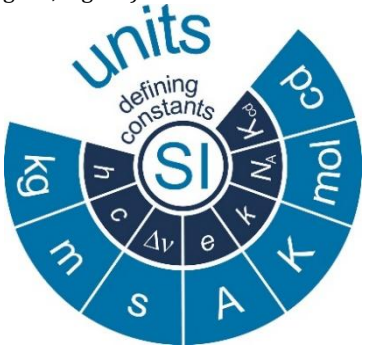

Fig. 13. Units and defining constants of the revised SI [64].

Proposals for the definitions of the units of the revised SI were published [22]. Here we will compare the current and the proposed new definition for the metre and the kilogram only. Whereas for the metre definition just the wording is modified to be aligned with the so-called explicit constant formulation, the definition of the kilogram changes completely:

Existing definition of the SI unit of length:

The metre is the length of the path travelled by light in vacuum during a time interval of 1/299 792 458 of a second.

Proposed definition of the unit of length in the revised SI:

The metre, symbol m, is the SI unit of length. It is defined by taking the fixed numerical value of the speed of light in vacuum c to be 299 792 458 when expressed in the unit m s^{-1}, where the second is defined in terms of the caesium frequency $\Delta\nu_{Cs}$.

Existing definition of the SI unit of mass:

The kilogram is the unit of mass; it is equal to the mass of the international prototype of the kilogram.

Proposed definition of the unit of mass in the revised SI:

The kilogram, symbol kg, is the SI unit of mass. It is defined by taking the fixed numerical value of the Planck constant h to be 6.626 070 040 × 10^{-34} when expressed in the unit J s, which is equal to kg m^2 s^{-1}, where the metre and the second are defined in terms of c and $\Delta\nu_{Cs}$.

Please note that the specified numerical value of h in the proposed definition above is taken from the 2014 CODATA adjustment (uncertain digits marked in grey; $u_r = 1.2 \times 10^{-8}$). The numerical value of h will be fixed without uncertainty when the revised SI is put into place, taking into account published results of precision experiments for determination of h.

The analysis of the measurement results is performed by the Task Group on Fundamental Physical Constants of CODATA, the Committee on Data for Science and Technology of the International Council for Science. There will be an adjustment of the constants to provide the final values for the revised SI expected to take place in September 2017 with a final decision by CGPM in 2018. To be considered for use in this adjustment, new measurement results, for all constants relevant to the redefinition, must be accepted for publication by 1 July 2017 [38].

Fig. 14 exemplarily illustrates the explicit constant definition of the kilogram in the revised SI.

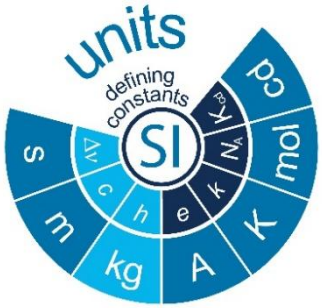

Fig. 14. Illustration of the explicit constant definitions in the revised SI, highlighted for the definition of the kilogram.

The proposed revision of the SI with its approach to define the SI units by fixing the numerical value of constants offers opportunities for the realization of the units in different ways using different experimental approaches, which will be described in detail in new *mise en pratique* documents, see chapter 4. This allows for key comparisons making the realizations less correlated, more stable and reliable.

The revised SI also offers flexibility with respect to scales, which can be explained best by referring to the unit of temperature or of mass. In the current system the mass of the IPK defines the kilogram and thus prioritises the mass of 1 kg, in the revised SI small uncertainties can in principle also be reached for masses being much smaller or larger than 1 kg even down to atomic or molecular masses that can, for the first time, be directly realized e.g. by photon recoil experiments.

It should not be concealed, however, that the proposed revision of the SI had also been critically discussed in literature. However, as of now, the discussions have converged in the respective Consultative Committees (CCs) of the Metre Convention with final recommendations to be made by the Consultative Committee for Units (CCU) in September 2017 for the CIPM and the CGPM. Recent criticism concentrated on dimensionless units like the radian for the plane or phase angle [128, 153, 124, 129].

Some combinations of the defining constants are known very precisely, e.g. the so-called molar Planck constant $N_A \cdot h$. It can be expressed as $N_A \cdot h = (M_u\, c\, \alpha^2)/(2\, R_\infty) \times A_r(e)$ with M_u as the molar mass constant, c as the speed of light, both having fixed numerical values in the current SI, and α as the fine structure constant (with $u_r = 2.3 \times 10^{-10}$), R_∞ as the Rydberg constant (with $u_r = 5.9 \times 10^{-12}$)

and $A_r(e)$ as the relative atomic mass of the electron (with $u_r = 2.9 \times 10^{-11}$), all known very precisely today. Thus $N_A \cdot h$ is known with a relative uncertainty of $u_r = 4.5 \times 10^{-10}$ [130].

This opens the possibility to compare independent high precision determinations of N_A and h each with target uncertainties of below 2 x 10^{-8}, by calculating precise values for h from N_A experiments and vice versa.

This possibility has also been addressed by the CIPM Consultative Committee for Mass, CCM [30], which described prerequisites for fixing the numerical value of the Planck constant h to be used as the basis for a redefinition of the kg. These prerequisites are:

- 3 experiments for h with $u < 5 \times 10^{-8}$
- at least 2 independent methods
- all results in agreement within their uncertainties
- 1 experiment with $u < 2 \times 10^{-8}$

The two independent methods mentioned by CCM which could potentially provide experimental data for h with $u < 5 \times 10^{-8}$ or even $u < 2 \times 10^{-8}$ are the so-called Kibble balance or watt-balance experiments and the Avogadro experiment. Following the CCM approach, CCM and the CCU jointly published a roadmap with the necessary steps to prepare for a possible redefinition of the kg [32, 157].

In 2016 Dr. Bryan Kibble, the inventor of the watt-balance technique, passed away and it was decided by the CCU and the watt balance community to rename the watt balance as the Kibble balance. This name will be used throughout the rest of this paper.

4. Experiments for redefinition of the kilogram

The CIPM Consultative Committee for Mass (CCM) is nearing completion of a new *mise en pratique* associated with the new definition of the kilogram. Once finalized and agreed upon by the member states of the BIPM, this document will provide a concise summary of practical methods whereby the unit of mass can be realized in the revised SI.

The current draft *mise en pratique* of the kilogram [126] begins with the definition of the unit of mass in the revised SI given already in 3.2. The numerical value of the Planck constant h defines the magnitude of $J\,s$ in the SI and, in combination with the SI second and metre, implicitly defines the magnitude of a kilogram in the revised SI. The definition does not give preference to any particular experiment or particular range at which to realize a unit of mass. Rather, all methods are in principle acceptable, ranging in scale from the atomic to the astronomic. However, it is logical that the experiments which were used to determine h from the existing artifact kilogram will have the most immediate potential to become primary reference measurement procedures (referred to as "primary methods" in the *mise en pratique*). In the following, the basic two independent methods mentioned by the CCM in the *mise en pratique* will be described in detail, namely the **Kibble (watt) balance experiments** and the **Avogadro experiment**, also known as the 'silicon route to the new kilogram' [172].

4.1. Kibble balance experiments

A Kibble balance experiment measures the Planck constant h in terms of a kilogram sized mass artifact by using a modified electromagnetic compensation balance. The core of the experiment is a one-to-one comparison between the gravitational force $F_G = m \cdot g$ of an object of mass m accelerating with gravity g while resting on a mechanical balance pan, and the magnetic force $F_{EM} = B \times L \cdot I$ generated by a coil of wire of length L carrying an electric current I and suspended from the same balance pan in a magnetic field B. If it is desired to achieve the one-to-one comparison of these forces, the coil must be suspended from the mass pan so that the magnetic force is coincident with, but opposing the gravitational force, and such that all other off-axis forces and torques arising from the coil interaction with the magnetic field B are negligible. In order to understand how this balance of forces can eventually lead to the Planck constant, it is worth considering a brief history of the experiment.

Recall that the present definition of the SI unit of current is in terms of force, see 3.1. This definition was realised using a current balance which measured the force between two current carrying coils. This apparatus had the drawbacks that the force was small, the heat produced by the current had a detrimental effect on the balance and the dimensions of the coils had to be measured with high accuracy. Attempting to improve the SI realization of the Ampere at the National Physical Laboratory, Kibble proposed a different approach in 1976 [91] that avoided the direct measurement of B and L by adding a second mode of operation to the experiment. Introducing a velocity mode, where the coil is translated at a velocity v while recording the voltage U induced across the open circuit terminals, Kibble showed that the ratio of the voltage induced to the velocity of the coil translation U/v is equal to the product B x L. The two modes of operation, static or weighing mode and dynamic or velocity mode, can be combined to express a virtual balance of mechanical and electrical power via the Kibble equation $m \cdot g \cdot v = I \cdot U$. For clarity, the principle of the two mode operation of a Kibble balance is illustrated in Fig. 15.

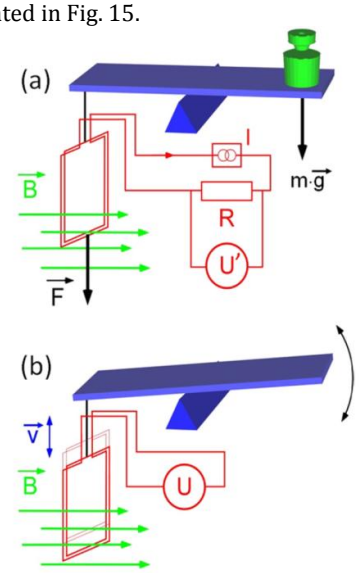

Fig. 15. Principle of Kibble balance: a) static and b) dynamic mode [55].

By combining the measurement of electrical power, obtained from the Kibble Balance, with a SI value of resistance, derived from a calculable capacitor, SI current or voltage can be measured.

In the late 1980's it became possible to measure the electrical watt, $I \cdot U$, in terms of quantum electrical standards. The laboratory or conventional electrical standards, as they have since come to be called, were established at this time [179] and are based on the quantum Hall Effect [187] for resistance and the Josephson effect [87] for voltage. The underlying physical phenomena in both devices depend on the unit charge e and the Planck constant h, with $U_J = hf/2e$ the Josephson voltage step and $R_K = h/e^2$ the quantum Hall resistance plateau, where f is the frequency of microwave radiation used to drive the Josephson junction to produce the voltage step. Measuring the current and induced voltage of a Kibble balance in terms of the quantum electrical standards, the Kibble balance relation becomes $m \cdot g \cdot v = K \cdot f_1 \cdot f_2 \cdot h$ where K is a known scaling constant, and f_1 and f_2 are the frequencies associated with the Josephson

voltage standards used as references to determine the current and the induced voltage. This form of the Kibble balance relation is easily solved for the Planck constant, and can be solved in a reciprocal fashion for a unit of mass using standards of time (frequency), length, voltage, and resistance all derived from fundamental constants once the kilogram is redefined. Of course for this to happen, Kibble balance experiments must achieve a combined relative standard uncertainty < 5 x 10^{-8}, a tremendous challenge given that the practical realizations of length, voltage, and resistance quantities have relative uncertainties themselves typically in the order of a few parts in 10^9.

The successful operation of a Kibble balance involves mastery of the realizations of several physical quantities and the integration of the primary measurement standards for these quantities as directly as possible into the measurement apparatus. The goal is to achieve an overall execution of the experiment such that the final uncertainty is limited only by the root sum of the squares of the uncertainties of the realizations. Looking over the Kibble balance equation, we see that in order to solve for *h* one must know the mass of a kilogram in vacuum, the local acceleration of gravity, the velocity of the coil, the constant *K*, associated with resistance scaling, and two frequencies associated with the measurement of the induced voltage and the weighing current, respectively. Taking a rough accounting of these quantities and the relative standard uncertainties presently available from their primary realizations is illuminating. The relative standard uncertainty of a primary Pt-Ir mass standard as calibrated by the BIPM during the recent Extraordinary Calibrations [175] was in the order of 2 x 10^{-9}. A more realistic estimate for the uncertainty of a Pt-Ir standard available to a Kibble balance after a period of several months and transitions between air and vacuum is 7 x 10^{-9}, perhaps more. Comparisons between absolute gravimeters used to measure the acceleration of gravity at a Kibble balance site typically have relative deviations from a reference value in the order of 2 x 10^{-9} [135]. The use of interferometry to measure absolute displacement over a distance of tens of millimetres has been demonstrated with uncertainties as low as 1 x 10^{-11} m [100], which would yield a relative precision in measuring the displacement of the coil over an 80 mm travel of 1.25 x 10^{-10}. However, the coil velocity is measured and the system is subject to noise sources such as ground vibration leading to an expansion of the uncertainty to something more like 2 x 10^{-9}. The uncertainty associated with the frequencies measured during the two voltage determinations is negligible. However, each of the frequencies represents a voltage, the value of which has a relative uncertainty in the order of 1 x 10^{-9} [178] for a total of 2 x 10^{-9}. The voltage used to determine the weighing current is measured across a resistor, and this contributes a further uncertainty, so that the total associated with electrical quantities is realistically more like 6 x 10^{-9}. Taking the root sum of the squares of these contributions reveals that the best that can be achieved under these circumstances is 10 x 10^{-9}. It is somewhat breathtaking then to observe that the most recent estimate of the combined relative standard uncertainty of the National Research Council of Canada (NRC), previously the NPL Mk II, Kibble balance is a mere 18 x 10^{-9} [163]. Of course, being precision engineers, we must ask: where do the other 8 parts in 1 000 000 000 come from?

The uncertainty of a Kibble balance experiment depends on numerous factors and is influenced by myriad design and manufacturing choices. Results from five very different balances can be found in the literature [163, 166, 55, 58, 181], and in anticipation of a redefined unit of mass several new instruments are in various stages of completion [78, 13, 94, 176, 194] as illustrated in Fig. 16.

For the purpose of this remaining discussion, rather than examine a specific error budget for a completed instrument in any detail, see e.g. [164], we will step back and view these Kibble balance experiments as a more general problem in instrument design as it applies to the pursuit of ultra-low relative uncertainties across this exciting landscape of instrument construction.

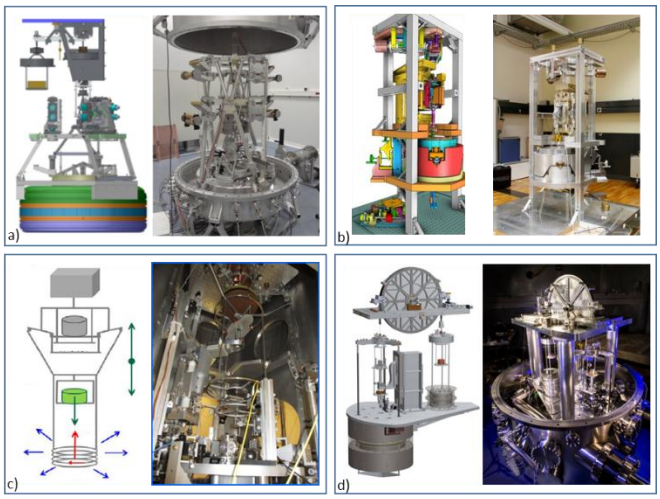

Fig. 16. New Kibble balances around the world a) LNE b) METAS c) BIPM d) NIST-4.

A conventional Kibble balance experiment is built completely around an electromagnetic compensation balance instrument that operates in two primary modes, weighing and velocity. These modes are combined to measure a value of the Planck constant, or, vice versa, to determine the magnitude of an arbitrary gravitational mass. In either application, one instrument must both weigh with precision and translate with precision subject to the constraint that the product *B x L* be predictable between the two operating modes. The form of a Kibble balance thus emerges from consideration of these two modes subject to this central constraint.

Consideration of the static mode of a Kibble balance instrument suggests that first and foremost it must function adequately as a mass balance. The instrument must be able to distinguish the mechanical force caused by a mass resting on the balance pan from all other forces acting on the balance. At a minimum, the static mode must faithfully resolve differences in the mass of its working standard at a level below 5 µg. In contrast, consideration of the dynamic mode suggests that this same instrument must also be capable of translating a wound wire coil affixed to the balance pan through a magnetic field in a highly controlled and repeatable fashion. A possible goal is to move the coil along the gravitational axis, and to simultaneously record both the velocity of the coil and the induced voltage. Ultimately, the ratio of voltage to velocity during the dynamic mode must provide a determination of the magnetic product *B x L* that is accurate, with a standard relative uncertainty below 5 parts in 10^9.

The constraint that *B x L* measured during the dynamic mode be predictable from the *B x L* responsible for the electrical force during weighing mode is a considerable challenge faced by Kibble balance designers. In conventional two mode balances changes in $B \times L$ may be caused by temperature changes, mechanical changes or magnetisation of the yoke by current in the coil. Extreme care must be taken to eliminate such changes from the measurements. To minimize these effects very different approaches, shown in Fig. 16, are employed by groups around the world.

Kibble and Robinson revisited the fundamental theory of the Kibble balance analytically [93] and showed that, under very specific circumstances, the Kibble equation is exact even if the force generated by the coil is not vertical. For this to be true the

Kibble balance coil must act as a rigid body with six degrees of freedom moving through space, so that it has three orthogonal components (v_x, v_y, v_z) of its linear velocity $\boldsymbol{V}$ corresponding to displacements along coordinate axes x, y, and z, and three orthogonal components (ω_x, ω_y, ω_z) of its angular velocity $\boldsymbol{\Omega}$ corresponding to rotations θ_x, θ_y, and θ_z about each respective coordinate axis, as indicated by the subscripts. The z' coordinate axis is aligned along the gravitational normal, as shown in Fig. 17.

When a current I flows in the coil of Fig. 17, it is linked by a magnetic flux Φ producing electrical force $\boldsymbol{F} = F_x + F_y + F_z$ and torque $\boldsymbol{\Gamma} = \Gamma_x + \Gamma_y + \Gamma_z$ on the coil. These forces and torques are transformed by the geometry of the balance, and in equilibrium, balance the weight mg of the mass m placed on the mass pan:

$$mg = -I\left(\frac{\partial\Phi}{\partial x}\frac{\partial x}{\partial z'} + \frac{\partial\Phi}{\partial y}\frac{\partial y}{\partial z'} + \frac{\partial\Phi}{\partial z}\frac{\partial z}{\partial z'} + \frac{\partial\Phi}{\partial\theta_x}\frac{\partial\theta_x}{\partial z'} + \frac{\partial\Phi}{\partial\theta_y}\frac{\partial\theta_y}{\partial z'} + \frac{\partial\Phi}{\partial\theta_z}\frac{\partial\theta_z}{\partial z'}\right) \quad (1)$$

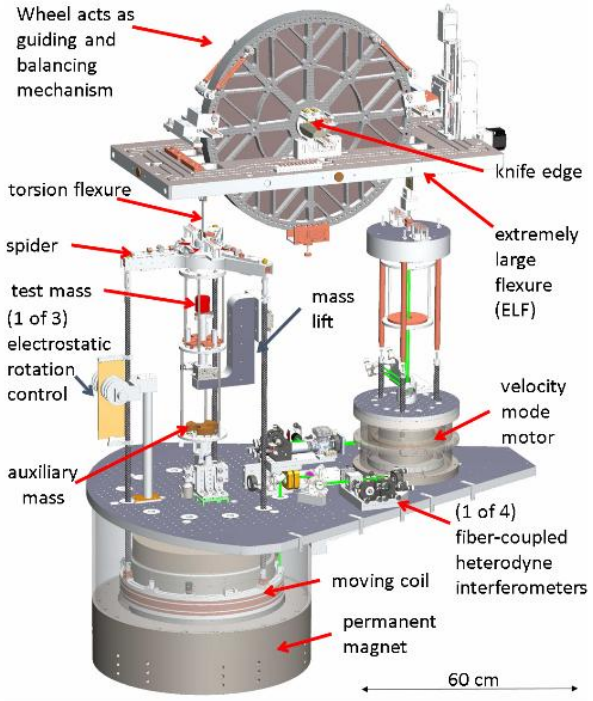

Fig. 17. Primary elements of a Kibble balance. The NIST Kibble balance uses the same device for balancing and guiding, a wheel supported at a knife-edge [79].

The current supply is disconnected, the coil is open circuited and moved with a general linear velocity $\boldsymbol{V}$ and angular velocity $\boldsymbol{\Gamma}$, a voltage U is induced across the open terminal pair, where

$$U = -\left(v_x\frac{\partial\Phi}{\partial x} + v_y\frac{\partial\Phi}{\partial y} + v_z\frac{\partial\Phi}{\partial z} + \omega_x\frac{\partial\Phi}{\partial\theta_x} + \omega_y\frac{\partial\Phi}{\partial\theta_y} + \omega_z\frac{\partial\Phi}{\partial\theta_z}\right), \quad (2)$$

Clearly, off-axis error motions of translation and rotation induce voltages. But, as it has been assumed that the motion of the coil is completely determined by the vertical motion of the mass pan $v_{z'}$ equation (2) can be rewritten:

$$U = -v_{z'}\left(\frac{\partial\Phi}{\partial x}\frac{\partial x}{\partial z'} + \frac{\partial\Phi}{\partial y}\frac{\partial y}{\partial z'} + \frac{\partial\Phi}{\partial z}\frac{\partial z}{\partial z'} + \frac{\partial\Phi}{\partial\theta_x}\frac{\partial\theta_x}{\partial z'} + \frac{\partial\Phi}{\partial\theta_y}\frac{\partial\theta_y}{\partial z'} + \frac{\partial\Phi}{\partial\theta_z}\frac{\partial\theta_z}{\partial z'}\right), \quad (3)$$

Combining equations 1 and 3 gives the Kibble equation

$$UI = mgv_{z'} \quad (4)$$

Assuming for the moment the magnetic flux and alignment of the coil with respect to the magnet are identical between the two modes, and so the expression is exact. This simplifies the construction and operation of Kibble balances but this depends on the exact cancellation of the bracketed terms in equations 1 and 3. This may be achieved using the rigid coil mountings described in [93] but is difficult to ensure in more conventional balances. Recently a construction and operation technique has been proposed which will extend and improve the insensitivity of any Kibble balance, having a common weighing and moving mechanism, to spurious forces and torques [160].

However, if the weighing and moving mechanism differ or there are effects, such as unwanted horizontal forces and torques which may generate small movements of the coil, this can prevent cancellation of the bracketed terms in equations 1 and 3 and then it is necessary to consider all terms in the virtual power equation

$$UI = \boldsymbol{F}\cdot\boldsymbol{V} + \boldsymbol{\Gamma}\cdot\boldsymbol{\Omega} \quad (5)$$

or

$$UI = \left(F_xv_x + F_yv_y + F_zv_z + \Gamma_x\omega_x + \Gamma_y\omega_y + \Gamma_z\omega_z\right) \quad (6)$$

Equation (6) gives a concise picture of the Kibble balance problem in such cases and is useful for assessing alignment uncertainties [74]. The measurand of interest among the terms on the right hand side of Equation (5) is the virtual mechanical powerF_zv_z, and the signal that is detected to represent this quantity is the virtual electrical power UI. Assuming that the voltage, current and velocity can be measured with sufficient accuracy, then in order for the product UI to represent F_zv_z with precision adequate for realization of mass, we must contrive a means to accurately measure each off-axis term and subtract it from the product UI, or we must construct the balance such that the ratio of each off-axis term to F_zv_z is less than a few parts in 10^8. In practice a combination of these two approaches is used. Here we will consider only the latter.

There are three ways to minimize the off-axis contributors to the measured virtual electrical power: (1) diminish the five off-axis forces, (2) diminish the five off-axis velocities, or (3) reduce both off-axis forces and velocities to diminish the off-axis product of Fv and then measure and compensate any that remain. For example, if

$$\frac{F_x}{F_z} = 10^{-4} \quad and \quad \frac{v_x}{v_z} = 10^{-5}$$

then,

$$\frac{F_xv_x}{F_zv_z} = 10^{-9}\,.$$

The magnitudes of the non-vertical forces and velocities can be minimized independently. The non-vertical forces depend on the respective gradients of the magnetic flux linkage. The off-axis x and y electrical forces, as well as all the electrical torques, can be minimized using symmetry in the magnet and coil. For a circular coil in a radial magnetic field, the flux gradients on opposing sides of the coil are symmetric and balanced, so that to first approximation the forces in the plane cancel. If the coil is also centered in the radial field, there will be no torques. The challenge, of course, is to construct and align the coil and magnet such that cancelation is complete and verify it by measurement. A perfectly radial magnetic field with a uniform vertical magnetic flux gradient is difficult to achieve, posing great challenges for the manufacturing of the pole pieces. For example, the magnet yoke for the Kibble balance being constructed at the BIPM is shown in Fig. 18, which includes a finite element model of the predicted field.

From the modeling, it was evident that machining tolerances at the level of 1 micrometre on cylindrical and planar surfaces with critical dimensions in the order of 200 mm or less would be required to achieve the necessary field uniformity [56]. Once machined, these parts were assembled using a dedicated device

capable of accurately positioning the heavy parts in the presence of very large magnetic forces, up to 10 kN, again while maintaining critical dimensions to within a few μm [5].

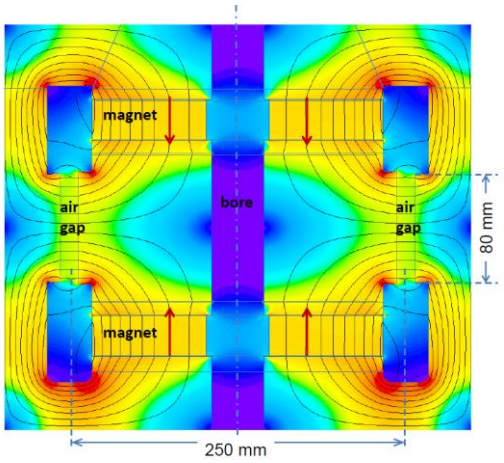

Fig. 18. Cross sectional view of the result of a finite element analysis of the magnetic circuit designed for the BIPM Kibble balance [56].

The accuracy achieved in the manufacture of the BIPM magnet is truly remarkable, yet relative uncertainties in the critical dimensions are still at the level of few parts in 10^5. Similar challenges occur in the manufacturing of the coil, where dimensional accuracy is even harder to quantify and maintain. Dimensional inaccuracy in these components of the order of a few parts in 10^5 will likely lead to similar variability of the vertical flux density, since there is a direct correlation between yoke, coil and field geometry. Even assuming that parts can be fabricated with relative geometric accuracies on the order of a few parts in 10^9, the magnetic properties of the materials might still be a limiting factor. Such magnetic properties can vary on the order of a few parts in 10^4, depending on how the magnet is assembled. Evidence of this type of variation was observed during final assembly and testing of the NIST-4 magnet system [169] where this perceived flaw was turned into a feature for "flattening" the field profile. In the end, residual asymmetries appear unavoidable in the construction and assembly of a realistic magnet and off-axis forces of the order of 10^{-4} F_z are likely in the as-built configuration. Further reduction is not completely hopeless, because asymmetries in the coil and magnet can fortuitously offset each other for certain orientations of the coil in the field; however, this requires precision mechanisms for adjusting the relative alignment of coil, magnet, and weighing axes and appropriate systems in place to measure and quantify the degree of misalignment [74].

The coil suspension on Kibble balances is typically constructed so that the coil orientation can be adjusted. In many balances, the suspension is also designed so that it only lightly constrains motions in the off-axis directions, a strategy employed by the two most successful Kibble balance experiments to date, the NIST (National Institute of Standards and Technology) and NPL/NRC instruments. As the coil is alternately energized and de-energized, the residual forces and torques experienced by the coil cause displacements of the coil from its static equilibrium that can be detected and measured. The orientation of the coil in the field is then readjusted in an attempt to minimize offsets.

On the new NIST-4 Kibble balance, for example, the coil has been suspended using a series of elements shown in detail in Fig. 19. Beginning at the wheel, a thin multi-filament titanium band rolls off in a tangent to the rim. This band transitions to a multi-filament cable that allows the lower elements to freely rotate in θ_z. The cable supports a dual gimbal flexure where both gimbals are free to rotate in θ_x and θ_y about the same center. The gimbal assembly supports both a rigid spider and the mass pan. Both the mass pan and spider are pendulums that share the same terminus, since the two gimbals are nested and have the same rotational center within manufacturing tolerances. The coil hangs off the rigid spider, suspended from three carbon fiber rods. The spider, rods, and coil create a cage-like frame with small flexure cubes at the joints, so that the structure can shear as a parallelogram along the x- and the y-axis (or any combination thereof).

After careful alignment, off-axis forces have been bounded to levels at or below a few parts in 10^5 of the on-axis load. Three orders of magnitude further reduction in the off-axis contributions to the total power must be established, leading to the consideration for diminishing the off-axis velocities.

Many recent designs address the functional requirements of translation and weighing using two separate mechanisms. The Swiss Federal Institute of Metrology (METAS) [13], BIPM [58], and Korea Research Institute of Standards and Science (KRISS) [94] use modified commercially available mass balances, or load cells, for the weighing mode, while the Laboratoire National de Métrologie et d'Essais (LNE) [181] use a flexure strip beam balance of their own design and manufacture. Regardless, these weighing instruments are null balance types where the load cell is intended to have a very limited range of motion and is optimized for weighing. The weighing instruments selected can all compare kilograms in a static configuration with resolution of a few micrograms, perhaps lower in a properly stabilized environment.

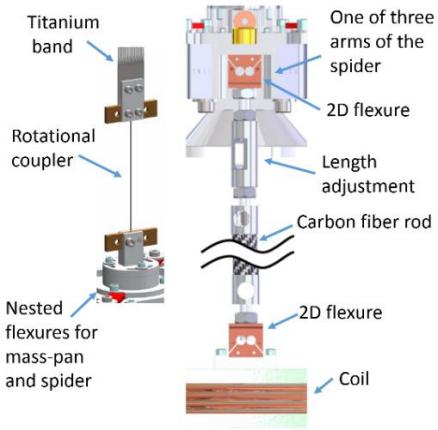

Fig. 19. The elements of the NIST-4 coil suspension [78].

In addition to the weighing instruments, these groups have designed auxiliary systems to translate the coil during velocity mode. For instance, at METAS a flexure stage has been designed, built and tested that will guide the translation of the weighing instrument, mass pan, and coil system as a single unit with respect to the fixed permanent magnet [42]. The flexure translation stage is driven using another counterbalanced flexure stage that compensates the static load of all the elements tethered below. The translation stage itself has demonstrated near flawless uniaxial translation over a range of 30 mm with straightness error below 100 nm and rotational errors below 10 μrad.

Similar approaches are employed at both LNE and KRISS to translate the entire weighing mechanism and coil with respect to the magnet. LNE uses a single counterbalanced flexure stage having 75 mm range of motion [188] that achieves the functionality of the combined METAS stages. Like METAS, KRISS employ a counterbalanced flexure system to handle the static load but use a novel journal bearing based on a piston gage as the uniaxial guiding mechanism [94]. In contrast to these approaches that move the entire weighing mechanism and coil with respect to the magnet, the BIPM translates the coil using a series of flexures

and linkages inserted as a serial linkage between the weighing instrument and the spider. The weighing instrument is stationary on a frame fixed to the magnet in this scheme, and the flexure linkage is actuated to expand and contract during velocity mode to achieve uniaxial coil motion.

The challenge for all approaches is to ensure that the weighing axis, electromagnetic axis, and translation axis are coincident and do not vary between velocity and weighing mode. Clearly, by employing a separate translation system, the groups discussed so far hope to minimize the off-axis velocity components during velocity mode. A question that remains is whether or not such ultra-precision translation stages yield uniaxial coil translations, and whether or not the translating coil axis is the same as the weighing axis. All these groups have developed means to test this hypothesis, but data is not yet available regarding the performance.

Kibble and Robinson [93] make a compelling case for creating an instrument where the balance mechanism and coil reduce to a single-degree-of-freedom. They advocate that next generation balances might be constructed as a rectilinear spring, much like the coil and suspension system of an inertial frame "super-spring" used in many absolute gravimeters. The idea is that if the coil and balance form a single coordinate axis, it will assure consistency between weighing and motion, and could in principle completely relax the need to minimize the off-axis flux gradients. Such a constrained design does not need extremely precise constraints on its motion, it just needs to ensure that changes in the bracketed terms in equation 1 and 3 do not change significantly between weighing and moving modes. The technique described in [160] makes this even easier to achieve

As an example of a single-mechanism approach, consider the NIST-4 Kibble balance, where the translation mechanism and weighing mechanism is a wheel that pivots on a knife edge bearing. A multi-filament band rolls off the wheel from which the coil is suspended using the spider and frame, just as previously discussed with respect to Fig. 19. The scheme allows the coil and mass pan to hang naturally along the gravitational axis and to self-align the weighing and translation axes, preserving the symmetry of the system even if the mass exchange is off center. In principle, for an absolutely sharp knife edge, the only deviation from a z translation will be due to variation in the radius of the wheel, which will translate the point of tangency from which the band rolls off the wheel. In order to achieve the necessary precision, the diameter of the NIST-4 wheel was turned on a high-precision diamond turning lathe. The roundness was measured by the NIST dimensional metrology group on a Coordinate Measuring Machine (CMM), as shown in Fig. 20.

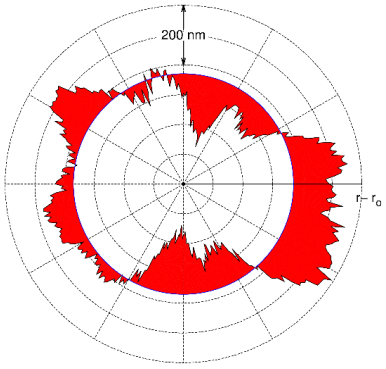

Fig. 20. Coordinate measurements of the NIST-4 balance wheel. The wheel has a nominal radius of 300 mm.

The diameter varies by less than 950 nm around the circumference, so that parasitic translations of the coil center due to wheel run out should not exceed ± 475 nm. The mechanism can achieve an 80 mm translation that takes 80 seconds. Assuming the diameter varies continuously from its smallest value to largest over 60 degrees of rotation implies a horizontal linear translation of about 250 nm over the full range of motion, which is about 15 degrees. This would suggest an error velocity of about 3 nm/s, which is still a relative error with respect to vertical velocity of 3.0×10^{-6}. In practice, off-axis velocities have been monitored and found to be closer to 80 nm/s, likely due to the finite radius of the knife edge.

4.2 The joule balance

The joule balance is closely related to the Kibble balance. Just as the Kibble or watt balance virtually compares mechanical to electrical power, both are measured in units of watt, the joule balance virtually compares mechanical to electrical energy, both of which are measured in units of joule. Energy is obtained by integrating power over time, and hence the joule balance equation may be derived by integrating the Kibble balance equation.

The joule balance was pioneered at the National Institute of Metrology (NIM) in China. To date, NIM is the only laboratory pursuing this type of measurement. The difference between the Joule balance and the Kibble balance is mostly in how the measurement is conducted and not so much in the instrument design. In principle, any Kibble balance can be operated as a joule balance and vice versa.

Similar to the Kibble balance, the joule balance measurement is performed in two modes. In force mode, a mass is weighed at two different vertical locations z_1 and z_2. The mechanical energy difference between these two locations is given by $mg(z_2 - z_1)$. The electrical energy difference of these two locations is given by $(\varphi(z_2) - \varphi(z_1)) \cdot I$, where I is the current in the coil and $\varphi(z)$ is the flux linkage of the magnet and the coil at vertical position z. In contrast to the Kibble balance experiment, where the derivative of the flux linkage with respect to z, i.e., $\frac{\partial \varphi}{\partial z}$ is measured, here the flux linkage is measured at two locations. The flux linkage can be obtained in two different ways.

In the original joule balance, first published in 2006 [193], the source of the magnetic field was an electromagnet. In this case, the flux linkage is given by $\varphi(z) = M(z)I_s$, where $I_s$is the current in the source coil and $M(z)$ the mutual inductance between the source coil and the moving coil. The mutual inductance is the ratio of the induced voltage in one coil divided by the rate of change of the current in the other. This is a generalization of the more widely known self-inductance, defined as the ratio of the induced voltage in a coil divided by the rate of change of the current in that same coil. To obtain the mutual inductance it is required to modulate the current in the source coil and measure this current as a function of time such that the time derivative of this current can be calculated. The second measurement that is required is the induced voltage in the other coil. This measurement is performed twice, with the moving coil at two positions, $z_1$and z_2. The difference in flux linkage can be obtained as $\varphi(z_2) - \varphi(z_2) = M(z_2)I_s - M(z_1)I_s$.

The second approach to measure the flux linkage is applicable when the source of the magnetic field is a permanent magnet. Here, the coil is moved from z_1 to z_2. The integral of the induced voltage is given by $\int_{t1}^{t2} U\mathrm{d}t = \varphi(z_2) - \varphi(z_1)$, if the position of the coil is z_1 and $z_2$at the time t1 and t2, respectively. So, instead of measuring the voltage and the velocity as it is done in the Kibble balance experiment, the coil is moved from one precise location to the other, while the integral of the induced voltage is measured. Typically, the integration of the voltage is performed numerically.

4.3 Review of h measurements

Fig. 21 shows the measurement results of the Planck constant that were conducted in the past four decades, with the current CODATA recommended value shown as the vertical black line. The reduction in uncertainty over the years is impressive [171]. Kibble conceived the idea of the watt balance in 1976 and it took ten years before precision measurements with a Kibble or watt balance were taken; the results were published in 1990.

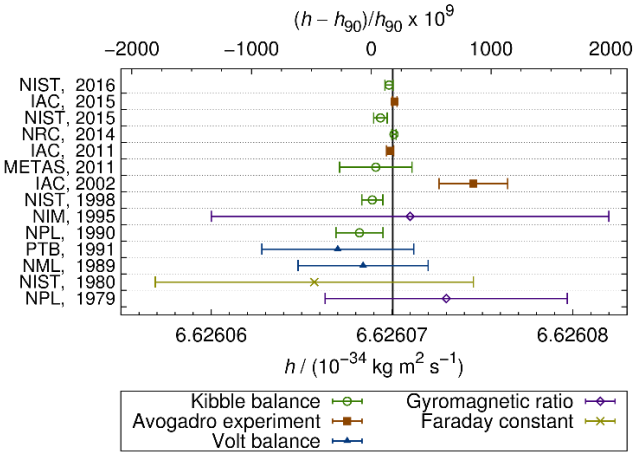

Fig. 21. Overview of measurements results of the Planck constant.

Before 1990 three different methods were used to measure the Planck constant: The gyromagnetic ratio, the volt balance, and the Faraday constant.

The gyromagnetic ratio of the proton is the quotient of the angular precession frequency of a proton in a magnetic field and the strength of the magnetic field. This quotient can be also expressed as the magnetic moment divided by the spin of the proton, $h/4\pi$. Since the magnetic moment of the proton can be compared to the magnetic moment of the electron, in a different experiment, the Planck constant can be obtained.

The volt balance compares the force between capacitor plates at different electrostatic potential to that of a mass in the gravitational field. The potential difference applied to the capacitor is compared to a Josephson voltage standard, which produces a voltage that is proportional to $h/2e$. Hence the voltage balance allows the determination of the Josephson constant $K_J = 2e/h$ in the SI. In order to obtain the Planck constant a second measurement is needed. One could use for example the fine structure constant α, which can be written as $\alpha = \frac{\mu_0}{16\pi}\frac{K_J^2 c}{h}$ with magnetic constant μ_0 and speed of light c and solve for h.

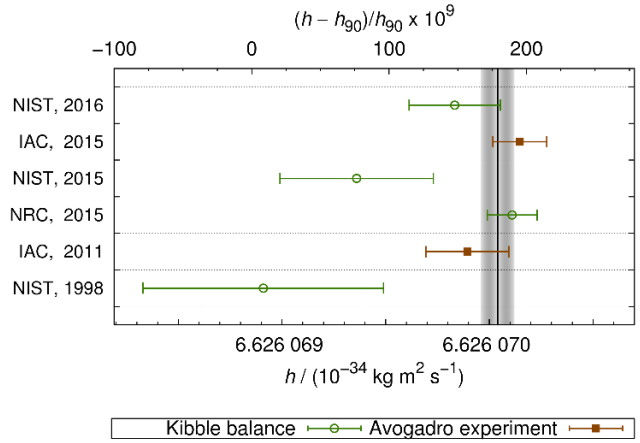

Fig. 22. High precision measurements of the Planck constant from Kibble balance and Avogadro experiments. The CODATA value from 2014 is shown as the vertical dark line. The vertical shaded area illustrates the standard uncertainty u of the adjusted value.

The Faraday constant is the product of the Avogadro constant N_A with the elementary charge e. As was addressed already in 3.2, a measurement of the Avogadro constant can be converted with a negligible increase in uncertainty into a value for the Planck constant. The value of the elementary charge can be eliminated with a measurement of the fine structure constant.

Since the late 90s, only measurements of the Kibble balance and the Avogadro constant produce competitive results for the measurement of h. Fig. 21 does not contain the NPL results reported in 2007 [158] and 2012 [159] as the 2014 NRC result was taken with the same apparatus after implementing essential improvements to eliminate the significant type-B uncertainties described in [159].

Fig. 22 shows the results that were used for the latest CODATA adjustment of h [130]. The CODATA value is given by the dark vertical line and the standard uncertainty is indicated by the grey shaded area. Even though, it appears that the data scatters more than it should, the results are statistically in agreement with more than 95 % confidence.

4.4. Avogadro experiment

The Avogadro constant N_A, named after the Italian scientist Amedeo Avogadro (1776-1856), is defined as the number of constituents (atoms or molecules) in a mole of a pure substance. It is thus a proportionality factor between the macroscopic world (e.g. mass of a mole of substance) and the atomistic world (molar mass of its constituent). Currently the mole is defined as one of the seven SI base units as 'the amount of substance of a system which contains as many elementary entities as there are atoms in 0.012 kilogram of carbon 12'. Within the revised SI the mole will be redefined by fixing the numerical value of the Avogadro constant N_A. The current draft definition is as follows [170]:

The mole, symbol mol, is the SI unit of amount of substance of a specified elementary entity, which may be an atom, molecule, ion, electron, any other particle or a specified group of such particles. It is defined by taking the fixed numerical value of the Avogadro constant N_A to be 6.022 140 857 × 10^{23} when expressed in the unit mol^{-1}.

Please note that the value of N_A specified in the above draft definition is based on the value from the latest CODATA adjustment from 2014: N_A = 6.022 140 857(74) ×10^{23} mol^{-1} with a relative standard uncertainty of 1.2 × 10^{-8}. In the revised SI the value for N_A will finally be fixed without uncertainty using the value of the CODATA adjustment based on the published measurement results until 1 July 2017.

Over the years, different methods were applied to measure N_A [14]. For example, Perrin was awarded the Nobel Prize in Physics in 1826 for his experiments of Brownian motion which confirmed the atomic nature of matter and which also provided values for N_A. Methods based on silver dissolution coulometry to determine the Faraday constant $F = N_A e$ gave a relative standard uncertainty of 1.3×10^{-6} also for N_A [25].

In 1963 Egidi proposed to use a pure and dislocation free crystal material as a possible new mass standard [54]. Measurements of the distances of the lattice planes (lattice parameters) and the macroscopic dimensions of a crystal sample thought of as a cube should also allow to determine the Avogadro constant. A way to measure the lattice parameters of bulk single crystal material was opened by the introduction of x-ray interferometers in 1965 [23], Deslattes first developed a combination of an x-ray and optical interferometer (XROI) which allowed to traceably calibrate crystal lattice spacings of silicon with small uncertainties below 10^{-6}, see Fig. 23 [51].

The so-called X-ray crystal density (XRCD) method for determination of the Avogadro constant with an uncertainty of about 10^{-6} has first been realised by Deslattes based on the formula below and using silicon single crystal material [52]:

$N_A = V_{mol} / v_{atom} = V_{mol} / (a^3/n) = n\,M / (\rho\, a^3)$

where $n = 8$ is the number of atoms per unit cell of a silicon crystal and ρ, M and a are the density, molar mass and lattice parameter, respectively.

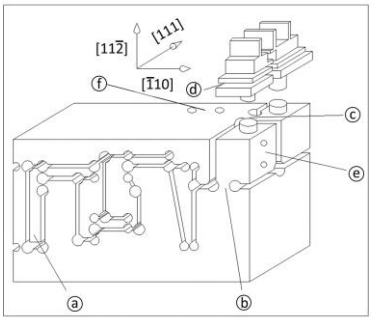

Fig. 23. Outline of principal parts of combined x-ray and optical interferometer. The optical mirrors (not shown) are attached to the main monolith brass structure (used for adjustment and fine translation) at e and f and form a cavity just above the x-ray interferometer. The symbols a, b and c denote flexures and d the silicon crystal x-ray interferometer [51].

A concept to use a quasi-perfect single crystal silicon sphere of about 93 mm diameter as a mass standard of 1 kg and possible replacement of the Pt-Ir prototype was first outlined by Zosi in 1983 [195]. The underlying equation can also be used to determine the Avogadro constant with small uncertainties if the macroscopic properties volume and mass of the sphere and its atomic properties lattice parameter and molar mass can be determined with sufficient uncertainty:

$$N_A = \frac{V_{sphere}}{v_{atom}} \cdot \frac{M_{mol}}{m_{sphere}} = \frac{V_{sphere} \cdot M_{mol}}{m_{sphere} \cdot \sqrt{8} \cdot d_{220}^3}$$

where V_{sphere} is the volume of the Si sphere, m_{sphere} is its mass, M_{mol} is the molar mass of the Si material, and d_{220} is the lattice spacing {220} of the Si crystal lattice, see Fig. 24.

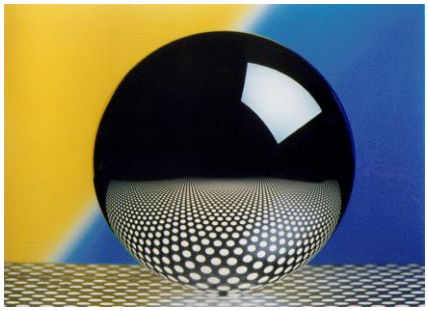

Fig. 24. Single crystal silicon sphere of 1 kg mass [courtesy PTB].

The proposal to use silicon as a suitable material for the Avogadro experiment was due to the experience gained in semiconductor industry in processing silicon as dislocation-free single crystal material with only very small amounts of impurities and excellent homogeneity. Zosi also already reflected on possible ways to cope with the different isotopic abundance in natural silicon (^{28}Si: 92.23 %; ^{29}Si: 4.67 %; ^{30}Si: 3.10 %): a) by enrichment of ^{28}Si until negligible traces of ^{29}Si and ^{30}Si are present or b) by determination of the ratios of the three isotopes by means of suitably calibrated spectrometers. The approach b), i.e. to use natural silicon has been followed first in the Avogadro experiments but it turned out that the achievable uncertainty for the molar mass is limited to $u_{rel}(M) \leq 3 \times 10^{-7}$ [15, 68]. It was thus decided to use isotopically enriched ^{28}Si material.

In 2003 the International Avogadro Coordination (IAC) project was established between five NMI's (Istituto Nazionale di Ricerca Metrologica (INRIM, IT), National Metrology Institute of Japan (NMIJ, JP), National Measurement Institute (NMI, AU), NIST (US), PTB (DE), the BIPM and the Institute for Reference Materials and Measurements (IRMM) of the European Joint Research Centre (JRC), which focused on manufacturing, processing and characterisation of isotopically enriched ^{28}Si material to further reduce the uncertainty for N_A. The approach has been concisely described in [127]: 'The international effort to determine the Avogadro constant, as described in the Metrologia special issue (Vol. 48, No. 2, April 2011), involved many tasks including the following: enrichment and polycrystal growth of silicon in the Russian Federation; growth and purification of a 5 kg single silicon crystal ingot in Germany; measurement of the isotopic composition of the crystals at PTB; measurement of the lattice spacing with the newly developed XROI described above at INRIM; grinding and polishing of two spheres cut from the ingot to nearly perfect spherical shape at NMI; optical interferometric measurement of the diameters of the spheres at PTB and NMIJ; measurement of the masses of the spheres in vacuum at PTB, NMIJ, and BIPM; and characterization of and correction for the effect of the contaminants on the surfaces of the spheres at various laboratories'. For a topical review of the IAC Avogadro project see [18].

The manufacturing process of the isotopically enriched ^{28}Si spheres started with the production of the ^{28}Si material. The isotope enrichment of SiF_4 was performed by gas centrifugation in Russia. The ^{28}Si polycrystal material grown by chemical vapour deposition (CVD) then was further handled by the Leibniz-Institut für Kristallzüchtung (IKZ) in Berlin to produce a single crystal ingot by a float-zone process, finished in 2007, see Fig. 25 [16].

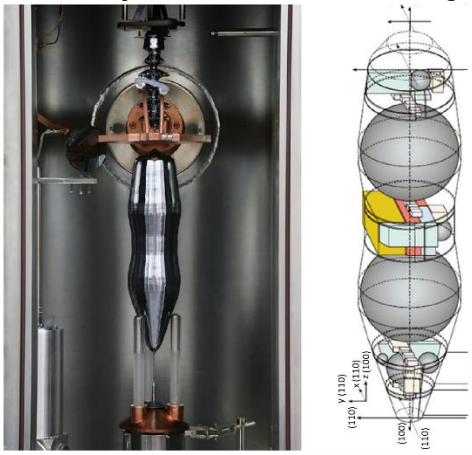

Fig. 25. The float-zone ^{28}Si crystal and its cutting plan. To determine density, two spheres (AVO28-S5 and AVO28-S8) were manufactured from the two bulges. To determine the lattice parameter, an x-ray interferometer was cut from the material between the two spheres (yellow part of the cutting plan). The enrichment is higher than 0.999 95 [2].

Fig. 25 shows the shape of float zone crystal and its cutting plan for further manufacturing of the Avogadro spheres, the x-ray-interferometer and several samples to characterise important properties of the enriched silicon crystal material.

For example, its impurities were characterized by infrared spectroscopy [191]. The influence of impurities and point defects (vacancy) on the crystal lattice parameter of the dislocation-free ^{28}Si single crystal material and its homogeneity were investigated by x-ray interferometry [112, 70]. The isotopic composition of the enriched material was determined by different methods [27] and gave the following results for the material of the spheres:

$x(^{28}\mathrm{Si}) = 0.999\,957\,50(17)$ mol/mol,

$x(^{29}\mathrm{Si}) = 4.121(15)\ 10^{-5}$ mol/mol,
$x(^{30}\mathrm{Si}) = 1.29(4)10^{-6}$ mol/mol.

The determination of the molar mass of the enriched material has been realized for the first time using a combination of a modified isotope dilution mass spectrometry (IDMS) technique and a high resolution multicollector-ICP-mass spectrometer, yielding a molar mass M('Si28') = 27.976 970 27(23) g mol^{-1} with a relative standard uncertainty $u_r(M('Si28')) = 8.2 \times 10^{-9}$ [148].

The manufacturing process of the two ^{28}Si spheres, cut out of the ^{28}Si ingot, was realised at the Australian Centre for Precision Optics (ACPO). The basic procedure was described in [101, 102, 103]. It consists of a) rough shaping using diamond tools and coarse loose abrasives (silicon carbide); b) fine grinding with loose abrasives (usually aluminium oxide) down to 1 µm; c) polishing using a matrix such as pitch with a suitable oxide slurry for finishing. A conical grinding tool rotating on a spindle and being designed for manual operation in a two calotte arrangement was used. The measured peak-to-valley (PV) diameter variations on the two spheres are shown in Fig. 26. It was found out later, however, that both spheres had unacceptable metallic contaminations by copper and nickel in their surfaces, due to the manufacturing process at ACPO.

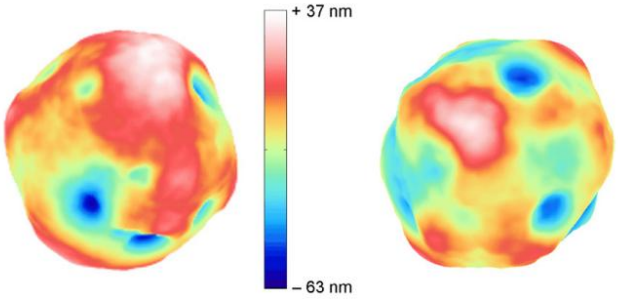

Fig. 26. Diameter topographies of the silicon spheres. Peak-to-valley distances are 98 nm (AVO28-S5, left) and 90 nm (AVO28-S8, right) [2].

By using a novel sphere manufacturing chain, which had been developed at PTB [116], the ^{28}Si spheres could be re-worked at PTB. An additional first etching step was applied to remove the metal contamination from the surfaces [7]. With the final polishing steps the PV diameter deviations furthermore were reduced down to 69 nm and 38 nm respectively, as shown in Fig. 27.

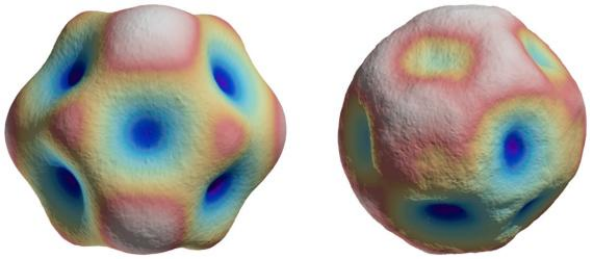

Fig. 27. Diameter topographies of the ^{28}Si spheres AVO28-S5c (left, PV = 69 nm) and AVO28-S8c (right, PV = 38 nm) [7].

The development of the complex manufacturing chain largely benefited from the measurement capabilities of PTB. Thus consecutive manufacturing and measurement procedures on the nanometre level were combined to ensure process control and repeatability [115, 138]. The manufacturing chain started with the Si ingot material, cutting cylinders using a diamond plated hollow drill. In a second step the coarse spherical shape was generated by single-point turning process on a lathe using a polycrystalline diamond insert as the cutting tool.

The subsequent lapping and polishing process steps were performed by means of a custom built manufacturing device based on a tetrahedron structure, see Fig. 28. The machine was designed and manufactured at PTB. A similar machine design in a simpler technical performance is known from the NASA Gravity Probe B experiment [4, 109].

Fig. 28. Lapping tools of the tetrahedron lapping and polishing device designed and used in the PTB manufacturing chain for Avogadro spheres [courtesy PTB].

The lapping processes employed different sizes of alumina grain (Al_2O_3) in aqueous solution. The laps were made of metal for the coarse grains and of glass for the fine grain size to use different material removal mechanisms and resulting removal rates. To cope with induced sub-surface damage, each step with a defined grain-size had to remove the damages induced by the previous step with larger grain-size. A removal of at least 5 times the diameter of the average grain of the previous process step was applied. The form deviation after fine lapping typically was less than 100 nm.

For the subsequent polishing processes, a medium hardness blend of commercially available optical polishing pitch was used [114]. First steps were performed with colloidal alumina polishing particles of about 1 µm size, while the finishing process used titanium dioxide nanoparticles of about 0.1 µm mean diameter in aqueous suspension with very low removal rates down to 1 nm/minute. Thus processing times of several weeks were generated. Furthermore, there was a negligible thermal input at the surface. The removal mechanism thus is assumed to be based on a local rheologically induced interaction on the atomic level, most likely similar to the mechanisms of other superpolishing processes, e.g. elastic emission machining or float polishing [116].

Fig. 29. Hollowed ingot, cut, turned, lapped and polished sphere [116].

Fig. 29 illustrates the different manufacturing steps for Avogadro spheres, which reliably yields Si spheres with approximately 93 mm diameter close to 1 kg mass, with roundness deviations around or even below 30 nm. No subsurface damage or contamination was observed and the ultrasmooth surfaces had average roughness values R_a about 0.2 nm with a very homogenous and stable SiO_2 layer of 1 nm -2 nm in thickness [115].

For the volume determination of the Si spheres V_{sphere} with a required target uncertainty of 0.3 nm for sphere diameter different optical concepts were realized. They are either based on Fizeau interferometry with plane waves or with spherical waves, see Fig. 30.

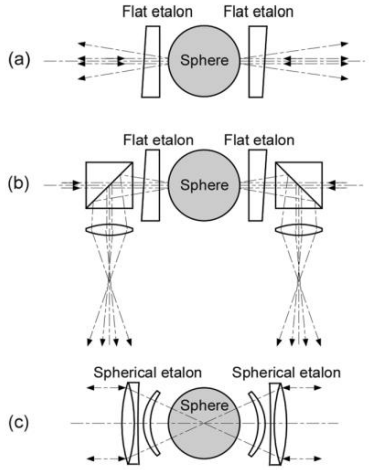

Fig. 30. Comparison of interferometers used to measure the diameter of spheres. (a) Optical configuration used in Saunders' interferometer, (b) that in the NMIJ interferometer and (c) that in the PTB interferometer [98].

A Saunders type interferometer [165] using plane waves was realised at NMIJ, see Fig. 31.

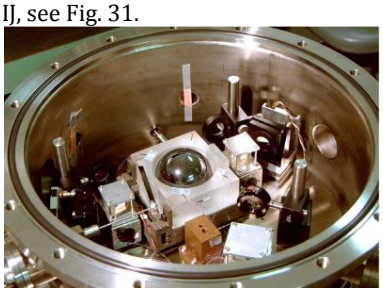

Fig. 31. Flat-etalon interferometer developed at the NMIJ [18].

With such a setup, one diameter can be determined from interferometric measurements for every position of the sphere within the Fizeau cavity [98]. An analysis of necessary phase corrections to the interferometric data was described in [3].

For a diameter mapping, the sphere thus has to be subsequently oriented in different angular positions for every interferometric diameter measurement. The volume is then determined from the measurement values of 280 diameters distributed nearly uniformly all over the surface of the sphere.

This is different for a spherical Fizeau interferometer, in which spherical wavefronts propagate to the surface of the sphere. In this case the interferogram provides information about a manifold of sphere diameters within the aperture of the spherical Fizeau objective [137, 12], see Fig. 32 for the first sphere interferometer developed at the PTB.

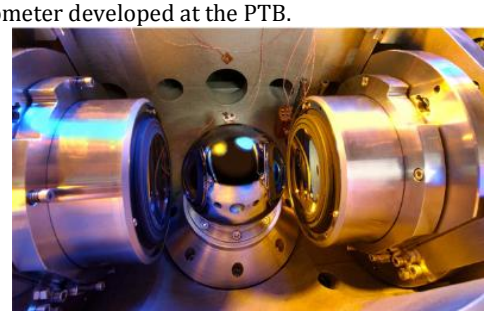

Fig. 32. Spherical-etalon interferometer developed at the PTB [18].

Fig. 33 shows a schematic view of the sphere interferometer. In every orientation of the sphere interferometric measurements are performed for the empty etalon and for the etalon containing the sphere. A tunable diode laser with a frequency range of 12 GHz emitting at 633 nm is used as the light source for the interferometer. It is stabilized to the target frequencies within a few 100 kHz, traceable to a HeNe iodine stabilized laser. The phase maps are calculated from five measured interferograms with phase steps of $\pi/2$ based on a phase-shifting technique [136].

The positioning system of the sphere consists of a lifting mechanism to remove the sphere from the Fizeau cavity and a two-axis rotation system for orientating the sphere. Within the 60° aperture angle of objectives about 10 000 diameters values can be measured in one orientation of the sphere. A full topography mapping of the sphere is realised by subsequent measurements in different orientations. Data evaluations were performed to take into account the distribution of measurement points on the sphere surface [9] and by using redundant information in the overlapping surface areas, also a radius (or absolute form) topography map can be reconstructed from the interferometric data [11].

Precise temperature measurement with sub-mK uncertainties, design considerations to limit disturbing thermal effects of actuators within the instruments as well tight thermal control of the environment of the Fizeau interferometer are crucial for achievement of small diameter measurement uncertainties due to the rather large coefficient of thermal expansion (CTE) of silicon of about 2.5×10^{-6} K^{-1}. Measurements of the CTE for the enriched ^{28}Si material were reported in [10]. Temperature measurements are referred to the International Temperature Scale (ITS-90) by use of temperature fix points (triple point of water (0 °C) and Gallium triple point (29.7666 °C)), which were used to calibrate Platinum resistance thermometers (Pt25) as references within the interferometer setup.

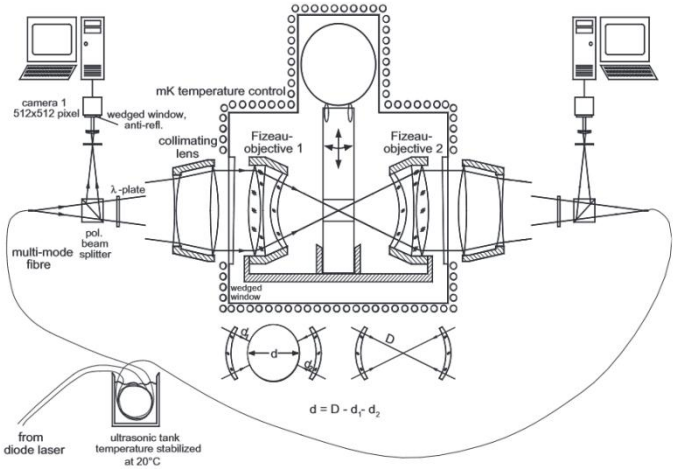

Fig. 33. Schematic view of the spherical interferometer [137].

To investigate unknown systematic differences in the spherical interferometer setup, a second independent version has been developed, which was designed differently concerning some of the optical components of the interferometer system, the instrument chamber and the positioning system of the sphere [107]. The achieved temperature stability of the water-cooled chamber walls is about 10 mK and the measured temperature stability inside the central part of the interferometer close to the sphere is about 1 mK/day. The aberrations of the new spherical Fizeau objectives with diameters of 10.16 cm (4") were specified to be $\lambda/50$ (for $\lambda \approx 633$ nm). Generally, the aberrations of the objectives and the form errors of the spheres superpose and result in interferometric retrace errors [108]. In addition to strive for high quality optical components with low aberrations also the further reduction of the topography deviations of manufactured Si spheres has been addressed.

Fig. 34 shows a topography map in Mollweide projection of the ^{28}Si sphere AVO28-S5c with a PV radius variation value of 46.8 nm, which was also shown in 3D representation in Fig. 27 left as diameter topography. The highly symmetric topography can be expressed as a rhombic dodecahedron and results from the varying elastic properties in different directions of the cubic Si crystal and application of a special polishing regime.

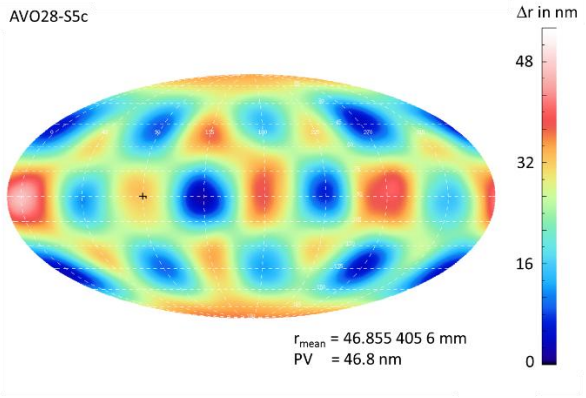

Fig. 34. Radius topography map of ^{28}Si sphere AVO28-S5c.

By variation of the polishing process on ^{nat}Si test spheres a further reduction of form error down to 16.7 nm PV radius variation could be achieved, however the underlying crystal symmetry is no longer clearly visible then, see Fig. 35.

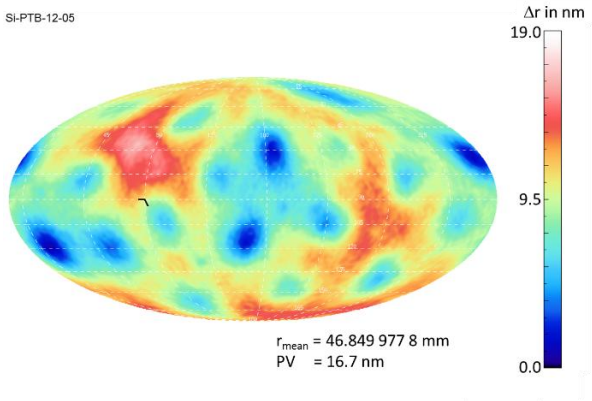

Fig. 35. Radius topography map of ^{nat}Si test sphere Si-PTB-12-05.

Another approach to further reduce the topography deviations of the Si spheres was reported, which uses ion beam figuring techniques for targeted modification of the Si surface [6].

The characterization of the surface layers of the Si spheres was performed by several different techniques, namely analytical methods for composition and stochiometry analysis (XPS, XRF), and structural analysis methods (XRR, XRD, and ellipsometry) [28]. Fig. 36 exemplarily shows the results of a complete characterization of SiO_2 layer thickness variation of the ^{28}Si sphere AVO28-S8c after re-polishing at PTB by spectroscopic ellipsometry.

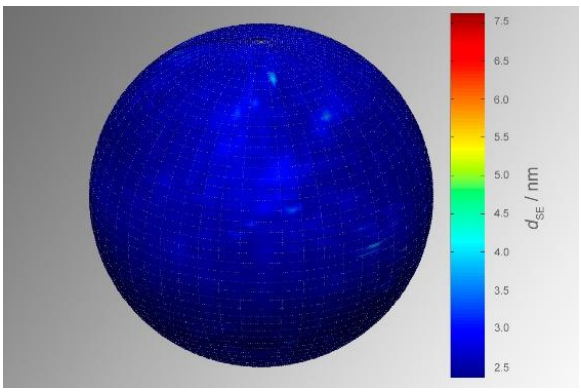

Fig. 36. Homogeneity of SiO_2 surface layer thickness on the ^{28}Si sphere AVO28-S8c, measured by spectroscopic ellipsometry [69].

The measurement results show a homogeneous layer thickness distribution with a mean value of d_{OL,SE_MW} = 2.71 nm and a standard deviation of 0.16 nm ($d_{OL,\,SE\_Min}$ = 2.30 nm, $d_{OL,\,SE\_Max}$ = 7.43 nm). After referring to layer thickness reference results provided by x-ray reflectometry (XRR) a mean value for the SiO_2 layer thickness of d_{OL} = 1.17 nm was determined with a standard uncertainty of $u(d_{OL})$ = 0.13 nm.

Following the pioneering work by Deslattes [51], the ^{28}Si crystal lattice parameter d_{220} was determined by a combination of an x-ray interferometer and an optical interferometer at INRIM. The result is d_{220} = (192 014 712.67 ± 0.67) am, at 20.0 °C and 0 Pa with a relative uncertainty of 3.5 x 10^{-9}. The measured d_{220} value is greater by 2 x 10^{-6} than the spacing in natural Si, a difference which confirms quantum-mechanics calculations [111]. Fig. 37 shows a schematic drawing of the setup.

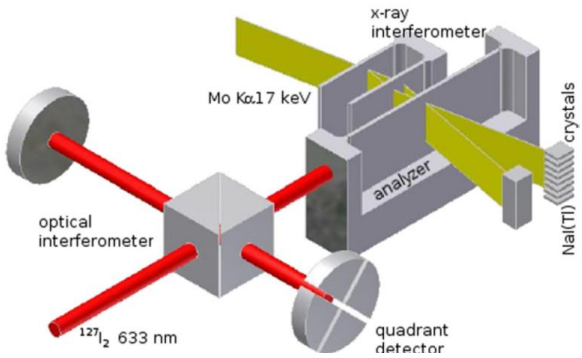

Fig. 37. The combined x-ray and optical interferometer. While the analyser crystal moves in a direction parallel to the laser beam, its displacement is measured by the optical interferometer and each passing diffracting plane is counted. Both the x-ray and optical interference patterns are imaged into position-sensitive detectors to sense lattice strain and parasitic rotations of the analyser [111].

It is known, that an x-ray interferometer can also be used to investigate nonlinearity interpolation errors of optical interferometers [143]. Fig. 38 shows the results of such investigations of a newly developed optical interferometer compared with the x-ray interferometer operated at NPL [189].

In addition to the procedures described above for precise determination of the molar mass, the lattice parameter, and the volume of the two spheres, the masses of the ^{28}Si spheres were determined on high-precision prototype balances operated at the BIPM and other NMI's [142].

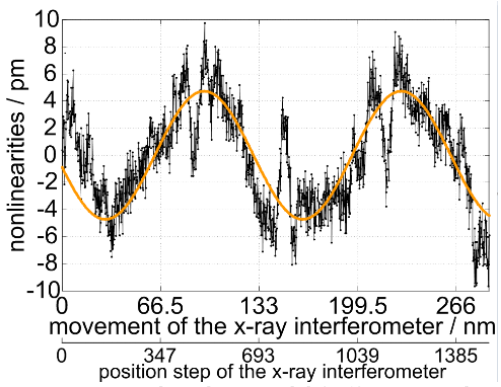

Fig. 38. Measurement result and sinusoidal fit (function with a period of 133 nm and an amplitude of 4.8 pm (solid line)) for the residual periodic non-linearity of an optical interferometer signal in comparison to the displacement measured by an x-ray interferometer [189].

The uncertainty of all measurement results of the IAC Avogadro project for N_A on the spheres which were contaminated with metal silicides was specified as 3 x 10^{-8} [2]. After decontamination and subsequent re-polishing of the spheres the relative uncertainty could be reduced to 2 x 10^{-8} [7]. Table 1 lists the major uncertainty contributions for the published value N_A = 6.022 140 76(12) × 10^{23} mol^{-1}. It can be seen, that the characterisation of the volume and the surface layers of the sphere provides the largest uncertainty contributions for N_A determination, i.e. precision engineering and dimensional metrology is still challenged. Recent ray-tracing simulations of the PTB sphere interferometers have shown, however, that the uncertainty contributions for the sphere volume measurements due to alignment influences of the optical system and the impact of the sphere's form deviation can be reduced.

Table 1. Major uncertainty contributions for the N_A value published for the sphere AVO28-S5c in [7].

Quantity	Relative uncertainty / 10^{-9}	Contribution / %
Molar mass (M)	5	6
Lattice parameter (a)	5	6
Surface characterization (m_{SL})	10	23
Sphere volume (V)	16	59
Sphere mass (m)	4	4
Point defects	3	2
Total	**21**	**100**

5. Experiments for redefinition of the kelvin

5.1 Background

The kelvin, unit of thermodynamic temperature, is currently defined as "*the fraction 1/273.16 of the thermodynamic temperature of the triple point of water*" [Taylor (2008)]. The triple point of water is the point where three states of water (liquid, vapour, ice) co-exist in equilibrium. In calibration laboratories around the world this condition is routinely achieved within specially manufactured triple-point-of-water cells made of borosilicate glass or quartz. The definition means that every temperature measurement in the world is a comparison against the temperature of the triple point of water, T_{TPW}.

In 2005, the definition was updated to state that the isotopic composition of the water should conform to the composition of the International Atomic Energy Agency reference material, the so-called Vienna Standard Mean Ocean Water (VSMOW) [82]. The current temperature definition is thus based on a property of a special substance. Today uncertainties for the realisation of the triple point of water can be achieved with a standard uncertainty u = 0.035 mK (u_r =1.3×10^{-7}) [174].

In alignment with the general approach of the revised SI to define the SI units by fixing the numerical values of natural constants, the unit of temperature in the revised SI is proposed to be based on the Boltzmann constant, k, as defining constant. The 2014 CODATA value is: $k = R/N_A$ = 1.380 648 52(79) × 10^{-23} J K^{-1} (u_r = 5.7×10^{-7}) [130], where R is the molar gas constant [130, 131].

Because of the universal applicability of statistical mechanics, there are many different physical systems that can be used to determine the Boltzmann constant. In each system the Boltzmann constant is directly involved in the expression relating the average energy of constituents of the system to the thermodynamic temperature. The strategy for determining k involves consideration of physical systems, which are especially simple to analyse. Traditionally these consist of statistical 'gases' which could be molecular gases, photon gases, or electron gases. A focus issue of *Metrologia* from 2015 addressed the different methods to determine k [190, 62].

Molecular gases: In an ideal gas, the distribution of atoms among available translational states is described by the Maxwell-Boltzmann distribution in which the average energy of a molecule is $\langle E \rangle = 3 \times \frac{1}{2} kT$ where the factor 3 arises from the 3 translational degrees of freedom of a gas atom. The behaviour of real monatomic gases approaches this ideal behaviour at low density.

Photon gases: The distribution of photons among available quantum states in a cavity whose walls are at a uniform temperature is described exactly by the Bose-Einstein distribution function and the spectral intensity of radiation within the cavity is described exactly by the Planck formula [145]. Real so-called blackbody cavities can be constructed which allow the internal radiation to be sampled externally with minimal (and calculable) deviation from the Planck formula.

Electron gases: The distribution of electrons among available quantum states in a 'free electron gas' is described exactly by the Fermi-Dirac distribution function. The random motion of valence electrons within a conductor is well-described in many circumstances as a free electron gas. Fluctuations around the equilibrium distribution result in transient imbalance of electrical charges which in turn result in a spectrum of voltage fluctuations described by the Nyquist Formula [83, 84, 139]. Measurements of the magnitude and spectrum of these fluctuations at a known temperature allow the inference of the Boltzmann constant.

Techniques for probing these 'gases' provide opportunities to determine k. Experiments on molecular gases offer the possibility of the lowest uncertainty, with acoustic gas thermometry (AGT) [132] likely to achieve the lowest uncertainty followed by dielectric constant gas thermometry (DCGT) [2015]. These two methods put high requirements on manufacturing and precision engineering and will be considered in detail below.

In a curious interdependence, temperature – particularly around room temperature – is critically important for precision manufacturing. So let us briefly examine the calibration and measurement uncertainties in the region around room temperature. However, to understand the results, one needs to understand that there are two fundamentally different requirements of practical temperature measurements.

The first requirement is simply that we all agree on the temperature: the International Temperature Scale of 1990 (ITS-90) achieves this admirably [150] and thus enables world-wide reproducibility in manufacturing process control. For example, the expanded calibration uncertainties U (k = 2) offered by PTB for a Standard Platinum Resistance Thermometer (SPRT) at the fixed points of the ITS-90 are: U = 0.1 mK at the triple point of

water and U = 0.25 mK at the Gallium melting point (29.7646 °C). Such small SPRT calibration uncertainties also allows achievement of small standard uncertainties for the temperature of silicon spheres for the Avogadro experiments of u = 0.62 mK (k = 1) at 20 °C [98].

The second requirement is that the temperatures T_{90} determined by following the procedures of ITS-90 are close to the true thermodynamic temperature, T [61]. ITS-90 is based on our best estimates of thermodynamic temperature made prior to 1990 and more recent research has established that the temperature estimates on which ITS-90 was based were in error by much larger margins than indicated by the uncertainty in ITS-90. For example, the ITS-90 estimate of the Gallium melting temperature appears to be approximately 4 mK too low [185], even though the calibration uncertainty according to ITS-90 is only 0.25 mK (k = 2). Over most of the range in which SPRTs are used (13.8 K to 961.8 °C) the T_{90} appears to be in error by many parts in 10^5, but appears to be thermodynamically correct at the level of 1 part in 10^4.

The difference between the two requirements highlights the fact that for precision engineering the most important feature is the reproducibility of temperature measurements. The change to ITS-90 from IPTS-68 caused a step change of about 5 mK for temperature measurements at 20 °C [150]. The differences in length of a 1 m steel line scale therefore differed by about 55 nm between the IPTS-68 and ITS-90 definitions of "20 °C". Because of the increasing importance of ultra-precision manufacturing, and the satisfactory nature of ITS-90, it is unlikely that a revised ITS will be published in the near future. Rather it is more likely that a set of corrections will be made available to allow users to estimate T as closely as possible based on measurements of T_{90}.

5.2 Acoustic gas thermometry

In the relevant temperature range, most of ITS-90 is built upon constant volume gas thermometry (CVGT) in which the temperature of a known amount of gas trapped in a known volume is determined from measurements of its pressure. Acoustic gas thermometry (AGT) offers lower uncertainty of measurement and was originally developed at NIST and NPL [146, 39]. The principle of AGT is to measure the limiting low-density speed of sound u_0 of a gas, which is expected to closely approximate the ideal gas formula:

$$u_0 = \sqrt{\frac{\gamma_0 kT}{m}}$$

Where γ_0 is the limiting low-density value of the adiabatic index of a gas, which is exactly $\frac{5}{3}$ for a monatomic gas. If u_0 is measured at T_{TPW}, in a monoatomic gas of known molecular mass, m, then the value of k may be inferred.

The recent revival of the technique is built upon a body of work in the 1980s by Moldover and Mehl [117, 118, 119, 131] who noticed that using spherical resonators, rather than cylindrical interferometers, offered possibilities to obtain extremely low uncertainty. The inference of u_0 involves three key factors: (a) measurement of the frequency of acoustic resonances; (b) knowledge of the shape and average radius of the resonator; and (c) calculation of eigenvalues of the different acoustic resonances to allow multiple modes to be used to estimate u_0. It is in (b) and (c) that ultraprecision manufacturing techniques have aided the lowest uncertainty estimates.

In the latest implementations of the technique, the acoustic resonators are simultaneously used as microwave resonators and deliberately manufactured with a quasi-spherical shape – typically a tri-axial ellipsoid – with elliptical distortions in the order of 1 part in 10^3. The tri-axial distortion lifts the degeneracy of the microwave resonances and allows measurements of three components of many microwave triplets [120]. The distortion also slightly affects the acoustic resonances, but if the distortion is known, the effect can be compensated for [121]. The critical advantage of the simultaneous measurement of microwave resonances is that they are relatively insensitive to the gas within the resonator and so allow an estimate of the dimensions of the cavity with uncertainties of just a few nanometres [122, 53].

However, in order to achieve low uncertainty, it is essential that the cavity be manufactured in the correct shape. This ensures that u_0 estimated from different acoustic resonances can be compared because the eigenvalues of the real resonator correspond closely to those calculated for the shape. Additionally, only if the shape conforms to the theoretically-expected shape will different microwave resonances infer the same value for the radius.

Thus the dispersion among the u_0 values from different acoustic resonances is a stringent test of the overall coherence between theoretical analysis and its experimental realisation. In the NPL-Cranfield resonator NPLC-2 the dispersion of results from six acoustic modes was characterised by an uncertainty $u(u_0) = 0.09 \times 10^{-6}$. Dispersion amongst the radius estimates inferred from different microwave resonances is less than ±10 nm [49].

There are several publications on the application of the AGT method for determination of k [62], including approaches using a cylindrical resonator [192, 106]. The lowest uncertainty estimate of k so far has been reported by NPL [49, 50].

5.2.1 Specification and Manufacturing

The resonator for the determination of k by the AGT method at NPL was manufactured at Cranfield University by high precision diamond turning supported by on-machine and external measurement systems. Initially, eight hemisphere blanks were manufactured, and after inspection, four hemispheres were selected for finishing. Fig. 39 shows the design and realisation of the tri-axial elliptical resonator, while Fig. 40 shows the configuration of one part of the resonator (hemisphere) mounted on the diamond turning machine.

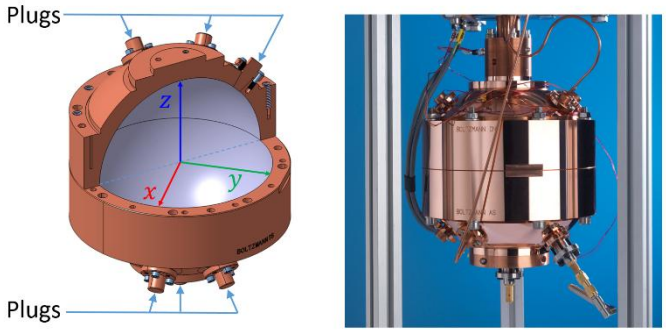

Fig. 39. Design and realization of the triaxial elliptical resonator used for the AGT method at NPL. Seven plugs allow the insertion of microwave antennas and acoustic transducers. These plugs initially protruded into the inner volume but were machined in place to match the local curvature of the ellipsoid.

The specific challenges for the manufacturing chain of the resonator hemispheres resulted from requirements to machine two tri-axial ellipsoids by non-rotationally symmetric (freeform) turning with sub-micrometre accuracy. The external cylinder was machined in the same cut as the inner surface to ensure that alignment of the external cylindrical surfaces on each hemisphere would result in alignment of the internal surfaces. Notice also the plugs which were machined in place.

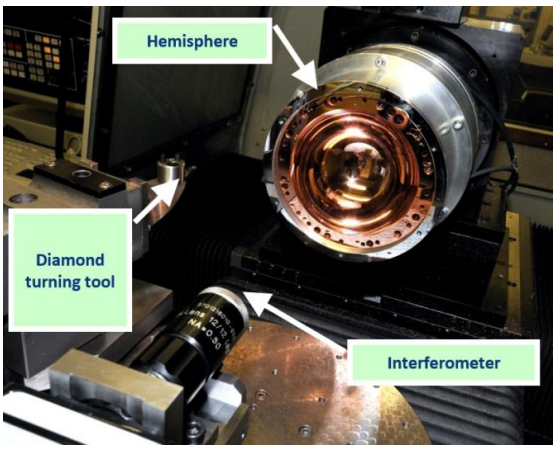

Fig. 40. Resonator hemisphere mounted on the diamond turning machine and monitored by on-machine interferometry.

For on-machine inspection of the processed surface an interferometer was used. Limitations regarding its field of view and fringe spacing required application of stitching interferometry to realize measurement of the full hemisphere. In between the machining steps, the hemisphere was measured on a CMM to check the machined radii in addition to its form. Because tactile CMM probing damages the sensitive surface of the copper hemisphere the final measurement was taken before the final machining pass, which removed < 2 µm from the Cu surface, see Fig. 41.

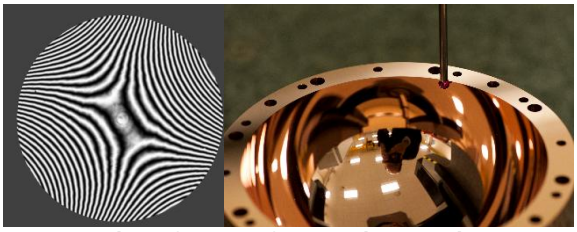

Fig. 41. Measured interferometer fringes and CMM probing.

5.2.2 Dimensional determination

The shape and average radius of the two NPL-Cranfield resonators (NPLC-1 and NPLC 2) was inferred from an analysis using three distinct measurement techniques. After receipt of the component hemispheres, the shapes of the internal resonator surfaces were measured using CMMs [48]. The resonators were then assembled and the internal volume of NPLC-1 was determined first by pycnometry with water and then with microwave spectrometry [184]. The volume and shape of NPLC-2 were then determined by microwave spectrometry [183].

5.2.2.1 CMM Analysis

The purpose of the CMM analysis was to independently assess the success of the manufacturing endeavour in a way that was directly traceable to SI base units. Prior to the measurements, the impact of the CMM probe on the copper surface was assessed by studying the damage pits created by probing at a range of contact forces and speeds [183]. Damage was observed under all conditions, but the minimum damage occurred using an 8 mm diameter stylus tip approaching at 1 mm s^{-1} with a contact force of 50 mN. The damage 'pit' caused by repeated probing under these conditions had a depth of approximately (45 ± 10) nm and a volume of less than one millionth of a cubic millimetre. Due to the damage to the copper spheres, the (x, y, z) coordinates of the point reported as being on the surface of the resonator will be in error by approximately (45 ± 10) nm in the direction of the normal to the surface. This will cause the resonators to be reported to be larger than they really are. We found no evidence of permanent marks on the steel, silicon, or Zerodur artefacts. There are also elastic effects which were corrected according to Puttock and Thwaite cases 1 and 4 [152].

The resonator hemispheres were placed on the CMM table alongside an ITS-90 calibrated capsule SPRT read by a resistance bridge, which recorded the temperature throughout all measurement operations with an uncertainty of ≈ 1 mK. In fact, the temperature in the room did not vary by more than 0.1 °C over several weeks required for the measurements. The shape and dimensions were measured against the calibrated CMM at several positions on the CMM table and the reported dimensions were compared with those of a silicon sphere whose average radius had previously been determined from density measurements.

The hemispheres were found to be within 1.5 µm of their design form and the point-cloud data from the analysis was inverted to allow estimates of the average radius and the volume of the assembled resonator.

5.2.2.2 Assembly and Microwave Analysis:

After CMM inspection, three blank plugs were removed and replaced with two carefully-constructed microwave antennas, and a port to remove the air. The spheres were then assembled by aligning the outer cylinders and the flat machined onto the rim. The degree of alignment was assessed by measurement on a Talyrond 295 *. After assembly, frequencies of microwave resonances were measured as the bolts connecting the cavity were tightened.

The shape of the cavity is designed to split triply-degenerate microwave resonances into three equally-spaced singlet resonances (Fig. 42). From the average of the singlet frequencies, it is possible to determine the average radius of the cavity, and from the differences between the singlet frequencies it is possible to determine the two principle eccentricities describing the cavity. However, the validity of these inferences depends critically on the degree of correspondence between the actual shape of the cavity and its theoretical shape.

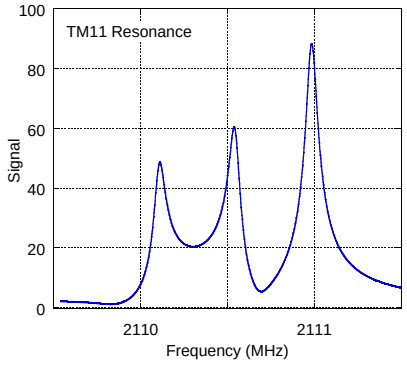

Fig. 42. The TM11 microwave resonance in the NPLC-1 resonator: The average frequency of the peaks is related to the average radius of the resonator. The splitting between the peaks is related to the eccentricity of the ellipsoidal inner volume.

The technique of microwave spectrometry includes the possibility of powerful self-consistency checking. The radius and eccentricities inferred by different microwave triplets have differing sensitivities to shape deformations, with higher frequency resonances being more sensitive to higher-order terms in a spherical harmonic multipole expansion of the resonator shape. Fig. 43 shows the average radius inferred from NPLC-2 with only two microwave antennas and a small port for gas

evacuation. The resonances cover the frequency range from 2 GHz to 20 GHz and the inferred radii a all lie within the range ± 3.9 nm ($u(a)$ = 2.2 nm: $u_r(a) = 0.035 \times 10^{-6}$). The consistency of these eight estimates indicates that the machined-shape is extremely close to the theoretically determined shape.

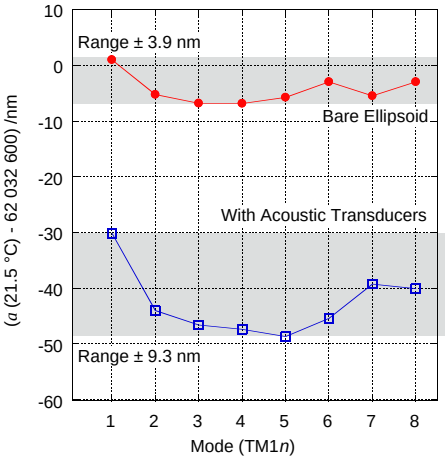

Fig. 43. The average radius a of the resonator inferred from the eight TM-modes with frequencies ranging from 2 GHz to 20 GHz. Each mode produces an independent estimate of average radius and the close agreement between modes is indicative of a close match between the theoretical target shape and that which was actually realised. The graph shows the differences in the radius estimates @21.5 °C from 62.0326 mm. A change of temperature by 1 °C would result in a change of radius of approximately 990 nm, a shift of 14 times the range of the graph.

Despite the internal self-consistency of the microwave results, it was still possible that a systematic error could have affected all radius and shape estimates and hence it was important to confirm the microwave measurements with conventional dimensional measurements – albeit at an uncertainty of comparison which was larger than the overall uncertainty of the microwave results.

A CMM study of the un-assembled hemispheres [183] encountered problems because of the lack of flatness of the flange, even though this amounted to only ±1 µm. In addition, the strain induced by bolting the hemispheres together further altered the assembled volume. This was monitored *in situ* using microwave spectroscopy and excellent agreement was found between finite element models and measured changes in the eccentricity of the resonator. After modelling the effects of compression upon the sphere and the flange, no significant disagreement was found between CMM and microwave measurements but the uncertainty of comparison was only $u(a)$ = 134 nm or $u_r(a) = 2.2 \times 10^{-6}$. A second test of the microwave results with lower uncertainty of comparison was thus desirable.

5.2.2.3 Pycnometry

The overall volume of the assembled resonator was checked by comparing microwave measurements with a pycnometric volume estimate in NPLC-1. To achieve this, it was necessary to use a liquid whose density is known to better than 1 part in 10^6: only two such liquids exist. The first is a particular sample of mercury characterised by Cook in 1957 [40, 41]: this was used for characterisation of the volume of the NIST resonator in 1986 [119]. The second is pure, de-gassed, isotopically-characterised water [177]. Mercury dissolves copper and so was not compatible with our quasi-spheres. However early tests showed that extremely still water reacts strongly with copper to yield a thick layer of black copper oxide. To avoid this NPLC-1 was first coated with benzotriazole. When coated correctly [105], this forms a self-stabilising 2 nm surface film which strongly resists corrosion by water.

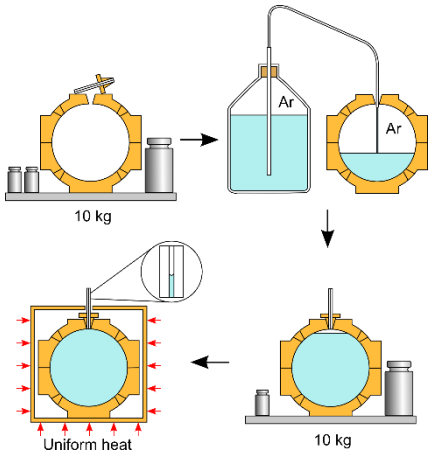

Fig. 44. The five-step procedure for the pycnometric volume determination.

After assembly and leak testing, the volume estimation consisted of five steps (Fig. 44). In the first step the empty resonator was weighed on a special 'tray' along with standard weights to bring the mass close to 10 kg. In the second step, the resonator was slightly under-filled with water, a procedure carried out under argon gas pressure resulting in partial saturation with argon gas. In the third step the filled resonator was weighed on its tray with weights to again bring its mass close to 10 kg. In the fourth step the resonator was heated by typically 3 °C until the liquid expanded sufficiently to fill the resonator to a fiducial mark in an attached glass capillary. The temperature at which this occurred was measured with an uncertainty of approximately 1 mK from which the density of water could be determined. Since the mass of the water was known from subtraction of the results of step 1 from step 3, the volume of the resonator could be determined.

The mass measurements were made using a Mettler AX64004 mass comparator, and consisted of repeated comparisons of our resonator and associated weights against calibrated 10 kg masses. The buoyancy of the copper resonator (approximately 1 g) was assessed by measurement of the pressure, temperature and humidity of the atmosphere within each enclosure on the comparator. To check this critical correction, weighings were carried out against both stainless steel and silicon standard weights for which the buoyancy correction differs significantly. After buoyancy correction, mass measurements had an uncertainty of < 1 mg.

Four volume estimates were made over a period of 4 months and were found to agree with a final radius estimate by microwave spectrometry with an uncertainty of comparison of $u(a)$ = 34 nm or $u_r(a) = 1.0 \times 10^{-6}$.

5.2.3 Summary

In NPLC-1, CMM, pycnometry and microwave measurements all resulted in consistent estimates of the average radius of the resonator, and no inconsistencies amongst these techniques were discovered. In NPLC-2, which could not be coated with benzotriazole, only CMM and microwave measurements were used to determine the radius of the resonator, and the final uncertainty in the radius determination was $u(a)$ = 12 nm or $u_r(a) = 0.19 \times 10^{-6}$. This low uncertainty, together with near perfect realisation of the desired triaxial form, was critical in achieving the overall low uncertainty of measurement of the Boltzmann constant.

5.3 Dielectric gas constant thermometry

The dielectric constant gas thermometry (DCGT) method has first been applied in the low-temperature region below 30 K to determine the density of Helium gas from dielectric constant measurements using the virial expansion of the Clausius-Mossotti equation [77]. The basic principle could be extended to larger temperature ranges. By measuring the dielectric constant ε of an (ideal) pressurized gas at a defined temperature T the Boltzmann constant k can be determined by using the following (simplified) relation:

$$p = kT(\varepsilon - \varepsilon_0)/\alpha_0$$

where p is the pressure, k is the Boltzmann constant, T the thermodynamic temperature, ε the dielectric constant of the gas, ε_0 the vacuum permittivity and α_0 the polarizability of the gas atoms (α_0 as proportionality factor between induced dipole moment p of an atom and the electric field E: $p = \alpha_0 E$).

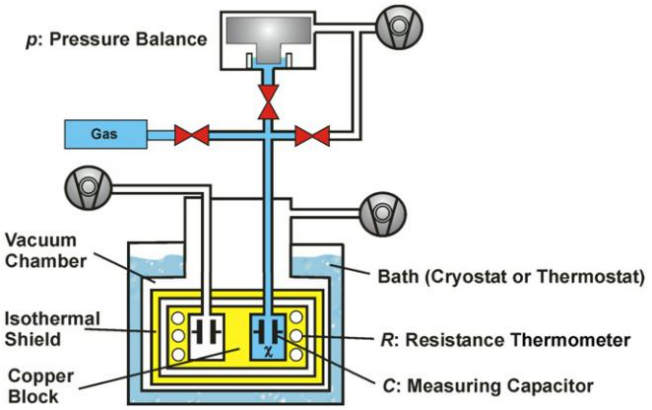

Fig. 45. Schematic of the DCGT experiment, realised at PTB [71].

The DCGT method has been realized at PTB to provide another independent measurement method to the already existing approaches for determination of k in preparation of the revised SI [59, 65]. Fig. 45 shows a schematic of the experiment.

In addition to the challenging requirements for the capacitive and temperature measurements also high precision pressure measurements are needed in order to achieve the targeted measurement uncertainties for k with the DCGT method of a few parts in 10^{-6}. The pressure measurements are traceable to dimensional calibrations of piston cylinder pressure gauges [43], which operate by floating a known mass on the piston which is free to rotate in the cylinder making use of the pressure difference resulting from the flow of medium (gas or liquid) through the clearance between piston and cylinder, typically about 1 µm.

Fig. 46. Piston cylinder pressure gauge system [courtesy PTB].

This operation principle requires high quality cylindrical components with small form deviations, which are usually made from tungsten carbide. Different pressures are realized by different effective areas of the gauge systems. Fig. 46 shows the basic components of such a piston cylinder pressure gauge which serves as a reference for realisation of the pressure scale at the PTB [162, 133].

For the DCGT experiment calibrated special pressure balances with piston–cylinder assemblies having effective areas of 2 cm^2 (7 MPa) and 20 cm^2 (0.75 MPa) were used. The dimensional characterisations were performed on different instruments for diameter and form calibration with optical and tactile probing, which necessitates the application of data fusion techniques to combine the measurement information from different instruments [88], see Fig. 47.

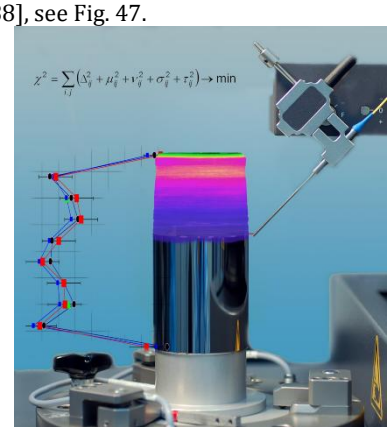

Fig. 47. Instrument for form measurements of a pressure gauge with an optical probe and visualisation of the data fusion process [courtesy PTB].

The diameter measurements were performed on a special Abbe length comparator which used two probes for contacting the cylinder surfaces. The probes were each mounted on a moving carriage guided in x-direction by an air bearing straight edge with interferometric position measurement of both carriages. The whole x-axis could also be moved in vertical direction to adjust to the designed measurement height on the cylindrical objects [134]. The overall uncertainty target of 1 x 10^{-6} for the calibration of the effective area of the pressure gauge system could be met, because the estimated uncertainties for the three-dimensional data points after data fusion were estimated as u = 8 nm (pistons) and u = 16 nm (cylinders) [89].

Fig. 48 shows published measurement results and their associated standard measurement uncertainties for k from the recent past for different measurement methods. Please note that the final result of the DCGT measurements at PTB with $u_r = 1.9 \times 10^{-6}$ is not included in the graph [72]. Aspects of the mise en pratique of the redefined kelvin were described in [60].

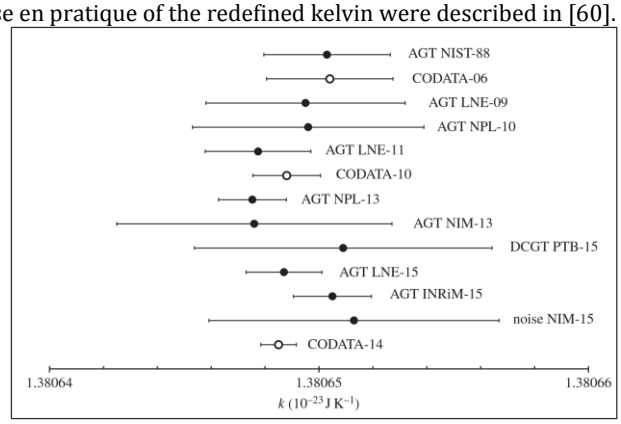

Fig. 48. Published values for the Boltzmann constant, which were used for the CODATA 2014 adjustment for k [63].

6. SI-units of electrical current, time, and luminous intensity

6.1 SI unit of electrical current

In the revised SI, the ampere will be defined by fixing the numerical value of the elementary charge e. The new definition is proposed as follows:

The ampere, symbol A, is the SI unit of electric current. It is defined by taking the fixed numerical value of the elementary charge e to be 1.602 176 620 8 ×10⁻¹⁹ when expressed in the unit C, which is equal to A s, where the second is defined in terms of $\Delta\nu_{Cs}$.

The best known value for e used in the above definition results from the CODATA alignment of different high precision electrical experiments. Progress in the determination of R_k, K_j, K_J^2 R_K and F could be obtained by experiments with Kibble or watt balances, coulometry, mercury electrometers, capacitor voltage balance experiments and determinations of the gyromagnetic ratio of particles (e.g. proton or helion) with a magnetic moment by frequency spectroscopy using the precession in a magnetic field. In addition, progress in the measurements of the fine structure constant α also improved the knowledge about R_K via the relation $R_k = h/e^2 = \mu_0\, c/2\alpha$ [127, p. 1558ff].

Since the conventional values $R_{K\text{-}90}$ and $K_{J\text{-}90}$ were fixed in 1990, substantial progress was thus achieved to reduce the uncertainty of R_K and K_J. The electrical measurements will be fully integrated into the revised SI, however with small step changes because the conventional values $K_{J\text{-}90}$ and $R_{K\text{-}90}$ will be replaced by K_J and R_K which will be set to exact values along with the fixing of the numerical values of h and e. The expected step changes are about 2×10^{-8} for resistance and 1×10^{-7} for voltage measurements [66]. The changes should only be visible to labs operating primary quantum standards; calibrations of even the most stable standard resistors and Zener diode references should be largely unaffected.

Another consequence of the revised SI will be that the magnetic constant μ_0 (permeability of vacuum) will no longer have the exact value of $4\pi \times 10^{-7}$ N A^{-2} but has to be determined experimentally. The value of μ_0 can be obtained with a relative standard uncertainty u_r, identical to that of the fine structure constant α from the exact relation $\mu_0 = \alpha\, 2h/(ce^2)$, which yields: $\mu_0 = 4\pi\,[1 + 0.0(2.3) \times 10^{-10}] \times 10^{-7}$ N A^{-2} [29, (update: CODATA 2014)]. The equation $\mu_0\, \varepsilon_0\, c^2 = 1$ follows from Maxwell equations.

Table 2. Relative standard uncertainties (in 10^{-8}) for some constants in the current SI and the proposed revised SI, based on the data published in CODATA 2014 [130].

Constant	Current SI	Revised SI	Constant	Current SI	Revised SI
m(K)	0	1.2	R	57	0
T_{TPW}	0	57	F	0.62	0
$M(^{12}C)$	0	0.045	σ	230	0
μ_0	0	0.023	K_J	0.62	0
ε_0	0	0.023	R_J	0.023	0
Z_0	0	0.023	$N_A\, h$	0.045	0
$\Delta\nu(^{133}Cs)_{hfs}$	0	0	m_e	1.2	0.033
c	0	0	m_u	1.2	0.045
K_{cd}	0	0	$M(^{12}C)$	1.2	0.045
h	1.2	0	α	0.023	0.023
e	0.61	0	J ←→ m^{-1}	1.2	0
k	57	0	J ←→ Hz	1.2	0
N_A	1.2	0	J ←→ K	57	0

Table 2 provides an overview of changes for different constants from the current SI to the revised SI system, showing that the uncertainty of the defining constants will be zero per definition in the revised SI. However, the mass of the IPK which is 1 kg exactly per definition in the current SI will have an associated uncertainty in the revised SI.

After redefinition of the SI, traceable current sources could in principle be realised by reliably generating and counting single electron events. A promising approach for a self-referenced single-electron quantized-current source has been described in [67]. The devices were manufactured by high resolution electron beam lithography techniques.

6.2 SI unit of time

Since 1967 the SI unit of time, the second, is defined as [35]:

The second is the duration of 9 192 631 770 periods of the radiation corresponding to the transition between the two hyperfine levels of the ground state of the caesium 133 atom.

For realization of this definition primary caesium atomic clocks are used, in which the frequency of microwave radiation (X-band) is stabilized to the Cs hyperfine transition. The relative uncertainties for realization of the second by means of Cs atomic clocks were continuously improved by about an order of magnitude every decade, see Fig. 49. A major step on this route was the development of so-called Cs atomic fountain clocks, in which laser-cooling is applied to slow down the Cs atoms and thus increase the interaction time with the microwave field.

Fig. 49 shows the development of the uncertainty of optical frequency standards over time, which surpass the trend of the Cs atomic clocks since about a decade. Different types of optical frequency standards have been developed using different atomic transitions, e.g. Yb^+ single ion or Sr atomic lattice clocks [75].

However, until now the optical clocks cannot yet compete with the established and more robust Cs atomic clocks regarding the time of continuous operation. It has therefore been decided that a redefinition of the unit of time based on a suitable clock transition in the optical range will not yet be part of the current revision of the SI proposed for 2018 [73].

The Consultative Committee for Time and Frequency (CCTF) of the CIPM has recently drafted a roadmap for the further developments, which are necessary for a future redefinition of the second based on a suitable optical clock transition [33]. This roadmap proposes five scientific-technical milestones to be reached before a possible redefinition of the second could then be put into force at the CGPM meeting in 2026 at the earliest.

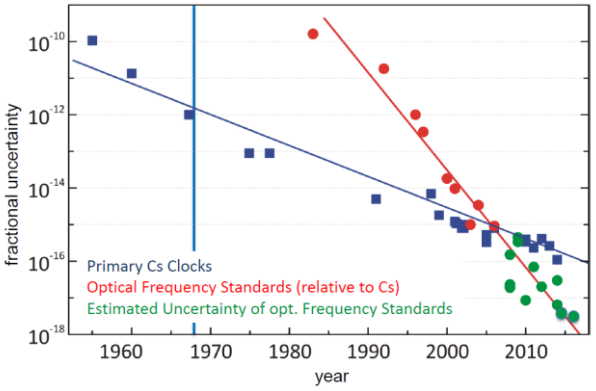

Fig. 49. Evolution of the fractional uncertainty of the realization of the second with caesium atomic clocks and of optical frequency standards. The vertical line indicates the time of introducing the current definition of the second [33].

6.3 SI unit of luminous intensity

The SI definition for the candela is radiant-based and as follows:

The candela is the luminous intensity, in a given direction, of a source that emits monochromatic radiation of frequency 540 x 10¹² hertz and that has a radiant intensity in that direction of 1/683 watt per steradian.

It should be noted that the frequency used in the above definition of the candela corresponds to a wavelength of 555 nm, where the spectral sensitivity of the human eye is at maximum. The proposed definition for the candela in the revised SI introduces the luminous efficacy K_{Cd} as the defining constant:

The candela, symbol cd, is the SI unit of luminous intensity in a given direction. It is defined by taking the fixed numerical value of the luminous efficacy of monochromatic radiation of frequency 540 × 10¹² Hz, K_{cd}, to be 683 when expressed in the unit lm W⁻¹, which is equal to cd sr W⁻¹, or cd sr kg⁻¹ m⁻² s³, where the kilogram, metre and second are defined in terms of h, c and $\Delta\nu_{Cs}$.

There are ongoing research activities to refer to quantum standards based on single photon counting for a future definition of the candela [196, 96]. Different approaches are followed to produce single photon sources and detectors [37]. One way is to use advanced micro- and nanofabrication techniques to realize epitaxially grown semiconductor quantum dots [26].

7. Activities in preparation of the revised SI

The scientific debate on a possible redefinition of the SI was intensively carried out over the last decades in literature and on scientific conferences [125]. During the last decade, draft documents for a possible redefinition and the corresponding *mise en pratique* documents were prepared by the consultative committees of the CIPM and published for discussion by BIPM.

During the last years, the communication to a wider scientific community and the general public as well on the revised SI commenced. Examples range from an educational publication on the determination of some of the defining constants of the revised SI with 1 % uncertainty by use of an Aluminium cube [44] over another one about a simple Kibble balance at 10 % uncertainty level [156] and the so-called LEGO watt balance developed at NIST [34] to a video discussion about the Kibble balance experiment [92].

Several approaches to the realization and dissemination of the kg in the revised SI are already published or under preparation [19, 149]. Also to be mentioned is the Helmholtz-Symposium 2016 [80] with an associated workshop 'Round and ready - Dissemination of the kg via Si spheres' [151] organized by PTB.

The CIPM also started an awareness campaign on the revised SI in 2015 for information of the wider public including educational institutions and publishers of educational books in Physics.

8. Conclusion and outlook

This keynote paper discussed the reasons and the outline of the envisaged redefinition of the International System of Units, called the revised SI. The proposed revision of the SI discards material artefact and dependencies on material properties and follows the path paved by the redefinition of the unit of time and, in particular length, the metre, back in 1983, namely to define an SI unit by fixing the numerical value of a fundamental constant. In the revised SI, the numerical values of the following natural constants will then be fixed: c, h, e, k, and N_A in addition to the fixed defining constants $\Delta\nu$ and K_{CD} for the unit of time, the second, and the unit of luminous intensity, the candela respectively.

This approach offers greater flexibility for different realizations and dissemination of the SI units and the derived units as well. An example is the future dissemination of the mass unit, which can either be realized by Kibble or watt balances or by calibrated Si spheres or via photon recoil experiments for atomic and molecular masses.

But how stable and universal are natural constants? Do they really provide a stable base for the SI? Experimental data from atomic clocks allowed to estimate a limit for the possible long-term drift of the fine structure constant α of $\Delta\dot{\alpha}/\alpha = -0.20(20) \times 10^{-16}$ per year or of the proton-to-electron mass ratio μ [81, 161]. Although a possible drift of α cannot be excluded, its possible instability is far too small to affect the acceptance of the SI system of units as a reliable foundation for science, industry and daily life. The revised SI will be reliable at the level of the uncertainties for realisation of the units. One of the decisive advantages is, that these uncertainties, in general, can be reduced to any level if technology proceeds without the need for redefinition. The only exception is the second which is open for further refinements, e.g. when it might be decided to base the time definition on optical clocks.

Precision manufacturing and precision engineering have been and still are indispensable enablers of progress in metrology, the science and application of measurement. It was described in this keynote contribution that without significant progress and support from precision manufacturing and precision engineering the basic measurement requirements for the revised SI could not have been fulfilled. It has also become clear that without in-depth knowledge in precision instrument design [85] making use of techniques like differentiation, symmetrisation, stabilisation and averaging the required measurement uncertainties of 2 x 10^{-8} and below could not have been achieved.

Acknowledgements

The valuable contributions from colleagues of STC P are gratefully appreciated, especially from W. Gao, A. Donmez, A. Archenti, W. Knapp, H. Haitjema, G. Goch, T. Estler, and C. Evans.

The advice and proofreading of parts of the manuscript by NMI colleagues involved in experiments for the revised SI is appreciated as well as the support of B. Przebierala (PTB) with some figures.

The authors would like to thank J. Ullrich (CCU president) for his recommendations and proofreading of the manuscript.

* **Note:** Certain commercial equipment, instruments, or materials are identified in this paper in order to specify the experimental procedure adequately. Such identification is not intended to imply recommendation or endorsement by the authors or their institutions, nor is it intended to imply that the materials or equipment identified are necessarily the best available for the purpose.

References

[1] Alder K (2002) The Measure of all Things—The Seven-Year-Odyssey that Transformed the World. *Abacus* London, ISBN 0-349-11507-9.

[2] Andreas B, Azuma Y, Bartl G, Becker P, Bettin H, Borys M, Busch I, Fuchs P, Fujii K, Fujimoto H, Kessler E, Krumrey M, Kuetgens U, Kuramoto N, Mana G, Massa E, Mizushima S, Nicolaus A, Picard A, Pramann A, Rienitz O, Schiel D, Valkiers S, Waseda A, Zakel S (2011) Counting the atoms in a 28Si crystal for a new kilogram definition. *Metrologia* 48: S1–S13.

[3] Andreas B, Ferroglio L, Fujii K, Kuramoto N, Mana G (2011) Phase corrections in the optical interferometer for Si sphere volume measurements at NMIJ. *Metrologia* 48: S104–S111.

[4] Angele W (1980) Finishing high precision quartz balls. *Precision Engineering* 2: 119-22.

[5] Arneson D, Liebers M, Knapp B (2014) Precision grinding components of a watt balance using a novel step-compensated conical hydrostatic work spindle. *Proc. 14th euspen International Conference*, 112-115.

[6] Arnold T, Pietag F (2015) Ion beam figuring machine for ultra-precision silicon spheres correction. *Precision Engineering* 41: 119-125.

[7] Azuma Y, Barat P, Bartl G, Bettin H, Borys M, Busch I, Cibik L, D'Agostino G, Fujii K, Fujimoto H, Hioki A, Krumrey M, Kuetgens U, Kuramoto N, Mana G, Massa E, Meeß R, Mizushima S, Narukawa T, Nicolaus A, Pramann A, Rabb SA, Rienitz O, Sasso C, Stock M, Vocke Jr RD, Waseda A, Wundrack S, Zakel S (2015) Improved measurement results for the Avogadro constant using a ^{28}Si-enriched crystal. *Metrologia* 52: 360–375.

[8] Barrell H (1962) The Metre. *J. of Contemporary Physics* 3, (1962), 415–434.

[9] Bartl G, Nicolaus A (2009) Influence of the distribution of measuring points on the mean diameter determination of the Avogadro project's silicon spheres. *Meas. Sci. Technol* 20, 6: 065104-1 - 065104-6.

[10] Bartl G, Nicolaus A, Kessler E, Schödel R, Becker P (2009) The coefficient of thermal expansion of highly enriched ^{28}Si. *Metrologia* 46, 5: 416 – 422.

[11] Bartl G, Krystek M, Nicolaus A, Giardini W (2010) Interferometric determination of the topographies of absolute sphere radii using the sphere interferometer of PTB. *Meas. Sci. Technol*. 21, 11: 115101-1 - 115101-8.

[12] Bartl G, Bettin H, Krystek M, Mai T, Nicolaus A, Peter A (2011) Volume determination of the Avogadro spheres of highly enriched 28Si with a spherical Fizeau interferometer. *Metrologia* 48: S96–S103.

[13] Baumann H, Eichenberger A, Cosandier F, Jeckelmann B, Clavel R, Reber D and Tommasini D (2013) Design of the new METAS watt balance experiment Mark II. *Metrologia* 50: 235–242.

[14] Becker P (2001) History and progress in the accurate determination of the Avogadro constant. *Rep. Prog. Phys.* **64** 1945–2008.

[15] Becker P, Bettin H, Danzebrink H U, Gläser M, Kuetgens U, Nicolaus A, Schiel D, De Bièvre P, Valkiers S and Taylor P (2003) Determination of the Avogadro constant via the silicon route. *Metrologia* 40 271–87.

[16] Becker P et al (2006) Large-scale production of highly enriched ^{28}Si for the precise determination of the Avogadro constant. *Meas. Sci. Technol*. 17 1854–60.

[17] Becker P, De Bièvre P, Fujii K, Gläser M, Inglis B, Luebbig H, Mana G (2007) Considerations on future redefinitions of the kilogram, the mole and of other units. *Metrologia* 44, 1–14.

[18] Becker P, Friedrich H, Fujii K, Giardini W, Mana G, Picard A, Pohl HJ, Riemann H and Valkiers S (2009) The Avogadro constant determination via enriched silicon-28 (Topical Review). *Meas. Sci. Technol*. 20 092002 (20pp).

[19] Bettin H, Schlamminger S (2016) Realization, maintenance and dissemination of the kilogram in the revised SI. *Metrologia* 53: A1–A5.

[20] BIPM (2016) Brief history of the SI. http://www.bipm.org/en/measurement-units/history-si (accessed 04.12.16).

[21] BIPM (2016) Mise en Pratique of the definition of the metre. http://www.bipm.org/en/publications/mises-en-pratique/standard-frequencies.html (accessed 04.12.16).

[22] BIPM (2016) On the future revision of the SI. http://www.bipm.org/en/measurement-units/new-si/ (accessed 04.12.16).

[23] Bonse U, Hart M (1965) An X-ray interferometer. *Appl. Phys. Lett*. 6:155–6.

[24] Borchardt L (1926) Längen und Richtungen der vier Grundkanten der großen Pyramide bei Gise. *Beiträge zur ägyptischen Bauforschung und Altertumskunde* 1, 1, Springer, Berlin.

[25] Bower VE and Davis RS, (1980) The Electrochemical Equivalent of Pure Silver - A Value of the Faraday. *J. Res. Natl. Bur. Stand*. 85, 175.

[26] Buckley S, Rivoire K and Vučkovic J, Engineered quantum dot single-photon sources. *Rep. Prog. Phys.* 75(12), 126503 (2012).

[27] Bulska E, Drozdov MN, Mana G, Pramann A, Rienitz O, Sennikov P and Valkiers S (2011) The isotopic composition of enriched Si: a data analysis. *Metrologia* 48 S32–S36.

[28] Busch I, Azuma Y, Bettin H, Cibik L, Fuchs P, Fujii K, Krumrey M, Kuetgens U, Kuramoto N, Mizushima S (2011) Surface layer determination for the Si spheres of the Avogadro project. *Metrologia* 48 S62–S82.

[29] CCEM/09-05 (2009) Draft *mise en pratique* for the ampere and other electric units in the (future) International System of Units (SI), http://www.bipm.org/cc/CCEM/Allowed/26/CCEM-09-05.pdf.

[30] CCM (2010) Recommendation G 1 Considerations on a new definition of the kilogram http://www.bipm.org/utils/common/pdf/CC/CCM/CCM12.pdf (accessed 04.12.16).

[31] CCM Recommendation to NMIs on managing the consequences of the corrections to the BIPM as-maintained mass unit (2015) http://www.bipm.org/cc/CCM/Allowed/15/17_agenda6&10_CCM-Recommendation.pdf (accessed 04.12.16).

[32] CCM and CCU joint roadmap towards the redefinition of the SI in 2018 (2014) http://www.bipm.org/utils/common/pdf/SI-roadmap.pdf.

[33] CCTF Strategy Document (2016) http://www.bipm.org/utils/en/pdf/CCTF-strategy-document.pdf.

[34] Chao LS, Schlamminger S, Newell DB, Pratt JR, Sineriz G, Seifert F, Cao A, Haddad D, Zhang X. (2014) A LEGO Watt Balance: An apparatus to demonstrate the definition of mass based on the new SI. arXiv:1412.1699v2.

[35] CGPM (1968) 13th meeting General Conference of Weights and Measures, resolution 1. http://www.bipm.org/utils/common/pdf/CGPM/CGPM13.pdf. (accessed 07.12.16).

[36] CGPM (2014) 25th meeting General Conference of Weights and Measures, resolution 1, http://www.bipm.org/en/CGPM/db/25/1/ (accessed 04.12.16).

[37] Chunnilall CJ, Degiovanni, IP, Kück S, Müller I and. Sinclair AG (2014) Metrology of single-photon sources and detectors: a review. *Optical Engineering* 53(8), 081910.

[38] CODATA http://www.codata.org/committees-and-groups/fundamental-physical-constants (accessed Jan 15, 2016)

[39] Colclough AR, Quinn TJ, Chandler TRD (1979) Acoustic redetermination of the gas-constant. *Proc. R. Soc.* Lond. 368, p. 125.

[40] Cook AH, Stone NWB (1957) Precise measurements of the density of mercury at 20 °C I: Absolute displacement method. *Phil. Trans. R. Soc.* London A 250, 978.

[41] Cook AH (1961) Precise measurements of the density of mercury at 20 °C II. Content method. *Phil. Trans. R. Soc.*London A 254, 125.

[42] Cosandier F, Eichenberger A, Baumann H, Jeckelmann B, Bonny M, Chatagny V and Clavel R (2014) Development and integration of high straightness flexure guiding mechanisms dedicated to the METAS watt balance Mark II. *Metrologia* 51 S88–S95.

[43] Dadson RS, Lewis SL, Peggs GN (1982), The Pressure Balance: Theory and Practice. *HMSO* London.

[44] Davies RS (2015) What is a Kilogram in the revised International System od units. *J. Chem. Educ.*, 92 1604 – 1609.

[45] Davis RS, Barat P, Stock M (2016) A brief history of the unit of mass: continuity of successive definitions of the kilogram. *Metrologia* 53: A12–A18.

[46] de Garis Davies N (1943) The Tomb of Rekh-mi-Rē' at Thebes. *The Metrolpolitan Museum of Art Egyptian expedition* Vol II, plate LXII.

[47] Delambe JP (1806) "Base du système métrique décimal"/Méchain, Delambre, Paris, Baudoin, 1806. (Rés. 1652(1)). Réserve. *Bibliothèque de l'Observatoire de Paris*. http://gallica.bnf.fr/ark:/12148/btv1b26001383/f4.item (accessed 04.12.16).

[48] de Podesta M et al. (2010) Characterization of the volume and shape of quasi-spherical resonators using coordinate measurement machines. *Metrologia* 47(5): p. 588-604.

[49] de Podesta M, Underwood R, Sutton G, Morantz P, Harris P, Mark DF, Stuart FM, Vargha G, Machin G (2013) A low-uncertainty measurement of the Boltzmann constant. *Metrologia* 50(4): 354–376.

[50] de Podesta M et al. (2015) Correction of NPL-2013 estimate of the Boltzmann constant for argon isotopic composition and thermal conductivity. *Metrologia* 52(5): p. S353.

[51] Deslattes RD (1969) Optical and X-ray interferometry of a silicon lattice spacing. *Appl. Phys. Lett.* 15(11), 386-8.

[52] Deslattes RD, Henins A, Bowman HA, Schoonover RM, Carroll CL, Barnes IL, Machlan LA, Moore LJ, and Shieldset WR (1974) Determination of the Avogadro constant. *Phys. Rev. Lett*. 33 463–6.

[53] Edwards G, Underwood R (2011) The electromagnetic fields of a triaxial ellipsoid calculated by modal superposition. *Metrologia*, 48(3): 114-122.

[54] Egidi C (1963) Phantasies on a natural unity of mass. *Nature* 200 61–2.

[55] Eichenberger A, Baumann H, Jeanneret B, Jeckelmann B, Richard P and Beer W (2011) Determination of the Planck constant with the METAS watt balance. *Metrologia* 48 133–141.

[56] Ellinghaus, JM, Arneson D, Brecher C, Kiss A, Knapp B, Lavergne T, Stock M, Wenzel C (2014) Fabrication of the Magnetic Circuit for the BIPM Watt Balance. *Proceedings ASPE 2014 Annual Meeting*, November 9-14, Boston, MA.

[57] Evenson, KM Petersen FR (1976) Laser Frequency Measurements, the Speed of Light, and the Meter. *Spectroscopy of Atoms and Molecules* 2, 349-368.

[58] Fang H, Kiss A, de Mirande E, Lan J, Robertsson L, Solve S, Picard A, Stock M (2013) Status of the BIPM Watt Balance. *IEEE Trans. Instr. Meas.*, 62: 1491-1498.

[59] Fellmuth B, Fischer J, Gaiser C, Jusko O, Priruenrom T, Sabuga W, Zandt T (2011) Determination of the Boltzmann constant by dielectric-constant gas thermometry. *Metrologia* 48, 382–390.

[60] Fellmuth B, Fischer J, Machin G, Picard S, Steur PPM, Tamura O, White DR and Yoon H (2016) The kelvin redefinition and its mise en pratique. *Phil. Trans. R. Soc. A* 374: 20150037.

[61] Fischer J et al. (2011) Present Estimates of the Differences Between Thermodynamic Temperatures and the ITS-90. Int J Thermophys (2011) 32:12–25.

[62] Fischer J (2015) Progress towards a new definition of the kelvin. *Metrologia* 52 S364.

[63] Fischer J (2016) Low uncertainty Boltzmann constant determinations and the kelvin redefinition. *Phil. Trans. R. Soc. A* 374 20150038.

[64] Fischer J, Ullrich J (2016) The new system of units. *Nature Physics* 12: 4-7.

[65] Fischer J, Fellmuth B, Gaiser C (2016) Wie viel Energie steckt in der Temperatur? Bestimmung der Boltzmann-Konstante. *PTB-Mitteilungen* 126 2: 89-97.

[66] Fletcher N, Rietveld G, Olthoff J, Budovsky I, and Milton M (2014) Electrical Units in the New SI: Saying Goodbye to the 1990 Values. *NCSLI Measure J. Meas. Sci.*, Vol. 9, No. 3, 30-35.

[67] Fricke L, Wulf M, Kaestner B, Hohls F, Mirovsky P, Mackrodt B, Dolata R, Weimann T, Pierz K, Siegner U, Schumacher HW (2014) A self-referenced single-electron quantized-current source. *Phys. Rev. Lett.* 112, 226803.

[68] Fuji F et al (2005) Present state of the Avogadro constant determination from silicon crystals with natural isotope compositions. *IEEE Trans Instrum. Meas*. 54 854–9.

[69] Fujii K, Bettin H, Becker P, Massa E, Rienitz O, Pramann A, Nicolaus A, Kuramoto N, Busch I and Borys M (2016) Realization of the kilogram by the XRCD method. *Metrologia* 53 A19–A45.

[70] Fujimoto H, Waseda A, Zhang XW (2011) Homogeneity characterization of lattice spacing of silicon single crystals by a self-referenced lattice comparator. *Metrologia* 48 S55–S61.

[71] Gaiser C, Zandt T, Fellmuth B (2015) Dielectric-constant gas thermometry. *Metrologia*, 52(5), p. S217.

[72] Gaiser C, Fellmuth B, Haft N, Kuhn A, Thiele-Krivoi B, Zandt T, Fischer J, Jusko O and Sabuga W (2017) Final determination of the Boltzmann constant by dielectric-constant gas thermometry. *Metrologia* 54 280–289.

[73] Gill P (2016) Is the time right for a redefinition of the second by optical atomic clocks? *Journal of Physics*: Conference Series 723 (2016) 012053.

[74] Gillespie AD, Fujii K, Newell DB, Olsen PT, Picard A, Steiner RL, Stenbakken GN, and Williams ER, (1997) Alignment uncertainties of the NIST watt experiment. *IEEE Trans. Instrum. Meas.*, 46(2).

[75] Grebing C, Al-Masoudi A, Dörscher S, Häfner S, Gerginov V, Weyers S, Lipphardt B, Riehle F, Sterr U, Lisdat C, (2016) Realization of a time-scale with an optical clock. *Optica* 3, 563-569.

[76] Guan Z, Herrmann K (2016) Geschichte der chinesischen Metrologie. Fachverlag NW, Carl Schünemann Verlag, Bremen, ISBN 978-3-95606-188-2

[77] Gugan D and Michel GW (1980) Dielectric Constant Gas Thermometry from 4.2 to 27.1 K. *Metrologia* 16 149.

[78] Haddad D, Seifert F, Chao L, Cao A, Sineriz G, Pratt J, Newell D, and Schlamminger S (2015) First measurements of the flux integral with the NIST-4 watt balance. *IEEE Trans. Instrum. Meas.*, 64(6).

[79] Haddad D et al. (2016) A precise instrument to determine the Planck constant, and the future kilogram. *Review of Scientific Instruments* 87:061301.

[80] Helmholtz Symposium (2016) The Realization of the Unit of Mass in the New SI. http://www.ptb.de/cms/presseaktuelles/messenevents/helmholtz-symposium.html (accessed 07.12.16)

[81] Huntemann N, Lipphardt B, Tamm C, Gerginov V, Weyers S, Peik E (2014) Improved limit on a temporal variation of m_p/m_e from comparisons of Yb+ and Cs atomic clocks. *Phys. Rev. Lett.* 113, 210802.

[82] International Temperature Scale of 1990 (ITS-90) - Technical Annex, Update Aug. 2013: http://www.bipm.org/utils/en/pdf/MeP_K_Technical_Annex.pdf.

[83] Johnson JB, (1927) Thermal agitation of electricity in conductors. *Nature*, 119, p. 50.

[84] Johnson JB (1928) Thermal agitation of electricity in conductors. Phys. Rev., 32, p. 97.

[85] Jones RV (1988) Some Considerations in Instrument Design. Chapter 9 in: *Instruments and experiences: papers on measurement and instrument design*, Wiley.

[86] Jones FE, Schoonover RM (2002) Handbook of Mass Measurement. *CRC Press*.

[87] Josephson BD (1962) Possible New Effects in Superconductive Tunnelling. *Physics Letters* 1, 251.

[88] Jusko O, Bastam D, Reimann H (2009) Tactile and optical cylinder calibrations with nanometer uncertainties. *Conf. Proc. ASPE*, 2795: 4 pages.

[89] Jusko O, Bastam D, Neugebauer M, Reimann H, Sabuga W, Prirurenrom T (2010) Final results of the geometrical calibration of the pressure balances to be used for the new determination of the Boltzmann constant. *Key Engineering Materials,* 437, 150 – 154.

[90] Key comparison data base: http://kcdb.bipm.org/. (accessed 07.12.16).

[91] Kibble BP, (1976) A measurement of the gyromagnetic ratio of the proton by the strong field method. in: *Atomic Masses and Fundamental Constants*, edited by J. H. Sanders and A. H. Wapstra (Plenum, New York, 1976), Vol. 5: 545-551.

[92] Kibble BP, Hartland T, Robinson I (2013) The Watt balance and redefining the kilogram. *NPL Internet-Video*: www.youtube.com/watch?v=VlJSwb4i_uQ.

[93] Kibble BP and Robinson IA (2014) Principles of a new generation of simplified and accurate watt balances. *Metrologia* 51 S132–S139.

[94] Kim D, Woo BC, Lee KC, Choi KB, Kim JA, Kim JW and Kim J (2014) Design of the KRISS watt balance. *Metrologia* 51 S96–S100.

[95] Kind D (2000) „Für alle Zeiten, für alle Menschen". *Physikalische Blätter* 56 Nr. 6: 63-66.

[96] Klein R, Thornagel R and Ulm G (2010) From single photons to milliwatt radiant power—electron storage rings as radiation sources with a high dynamic range. *Metrologia*, 47, 5, R33.

[97] Köbel J (1535) Geometrey, reprint 1598 online: http://digital.slub-dresden.de/fileadmin/data/265333075/265333075_tif/jpegs/265333075.pdf (accessed 04.12.16).

[98] Kuramoto N, Fujii K, Yamazawa K (2011) Volume measurements of 28Si spheres using an interferometer with a flat etalon to determine the Avogadro constant. *Metrologia* 48: S83–S95.

[99] Lambert R (2010) Economic impact of the National Measurement System: Evidence Paper July 2010. *Department for Business, Innovation and Skills*, https://www.gov.uk/government/uploads/system/uploads/attachment_data/file/297890/nms-economic-impact-evidence-paper-r-lambert-july-2010.pdf.

[100] Lawall, J and Kessler E (2000) Michelson interferometry with 10 pm accuracy. *Rev. Sci. Instrum.* 71, 2669.

[101] Leistner AJ and Zosi G (1987) Polishing a 1-kg silicon sphere for a density standard. *Appl. Opt.* 26 600–1.

[102] Leistner A, Giardini W (1991) Fabrication and Testing of Precision Spheres. *Metrologia* 28, 503-506.

[103] Leistner AJ and Giardini WJ (1994) Fabrication and Sphericity Measurements of Single-Crystal Silicon Spheres. *Metrologia*, 31, pp. 231-243.

[104] Lepsius R (1865) Die alt-aegyptische Elle und ihre Eintheilung. *Abhandlungen der königlichen Akademie der Wissenschaften zu Berlin*.

[105] Lewis G, Fox P G (1978) The thickness of thin surface films determined by photo-electron spectroscopy. *Corros. Sci.* 18(645–650).

[106] Lin H et al. (2011) Improved determination of the Boltzmann constant using a single, fixed-length cylindrical cavity. *Metrologia* 50(5): p. 417.

[107] Mai T, Bartl G, Nicolaus A, Peter A (2014) The new sphere interferometer for diameter determination of the Si-spheres for a redefinition of the kilogram. Fringe 2013: *Proc. 7th International Workshop on Advanced Optical Imaging and Metrology*, 863 – 866.

[108] Mai T (2016) Aufbau und Simulation des Kugelinterferometers II der PTB. (Dissertation) Technische Universität Braunschweig.

[109] Marcelja F, Keiser GM (1998) Silicon Spheres for Gravity Probe B Experiment. *Proc. of ASPE Spring Topical Meeting on Silicon Machining*, pg. 74-6.

[110] Marti K, Fuchs P, Russi S (2012) Cleaning of mass standards: a comparison of new and old techniques. *Metrologia* 49: 628–634.

[111] Massa E, Mana G, Kuetgens U, Ferroglio L (2011) Measurement of the {220} lattice-plane spacing of a Si x-ray interferometer. *Metrologia* 48 S37–S43.

[112] Massa E, Mana G, Ferroglio G, Kessler EG, Schiel D, Zakel S (2011) The lattice parameter of the Si spheres in the determination of the Avogadro constant. *Metrologia* 48 S44–S49.

[113] Maxwell JC (1870) Cambridge Lectures on Physics.

[114] Meeß R, Feist C, Löffler F (2013) Design and Validation of a Pitch Tester. *Proc. EUSPEN 13th Int. Conf.* Vol. II, 185-188.

[115] Meeß R, Felgner A, Hinzmann G, Lück A (2014) Surface topography of superpolished silicon spheres. *Proc. EUSPEN 14th Int. Conf.* Vol. II, 99-102.

[116] Meeß R, Hinzmann G, Lück A (2015) Improved manufacturing process chain for silicon spheres. *Proc. euspen's 15th International Conference*, 355-356.

[117] Mehl JB (1982) Acoustic resonance frequencies of deformed spherical resonators. *Journal of the Acoustical Society of America*, 71(5), p. 1109-1113.

[118] Mehl JB (1986) Acoustic resonance frequencies of deformed spherical resonators II. *Journal of the Acoustical Society of America*, 79(2), p. 278-285.

[119] Mehl JB and Moldover MR (1986) Measurement of the ratio of the speed of sound to the speed of light. *Phys. Rev. A*, 34, 3341–4.

[120] Mehl JB, Moldover MR, Pitre L (2004) Designing quasi-spherical resonators for acoustic thermometry. *Metrologia*, 41, p. 295-304.

[121] Mehl JB (2007) Acoustic Eigenvalues of a quasi spherical resonator: Second order shape perturbation for arbitrary modes. *Journal of Research of the National Institute of Standards and Technology*, 112(3), p. 163-173.

[122] Mehl JB (2009) Second-order electromagnetic eigenfrequencies of a triaxial ellipsoid. *Metrologia*, 46(5), p. 554.

[123] Mills IM, Mohr PJ, Quinn TJ, Taylor BN, Williams ER (2006) Redefinition of the kilogram, ampere, kelvin and mole: a proposed approach to implementing CIPM recommendation 1 (CI-2005). *Metrologia* 43, 227–246.

[124] Mills I (2016) On the units radian and cycle for the quantity plane angle. *Metrologia* 53:991–997.

[125] Milton MJT, Davis R, Fletcher N (2014) Towards a new SI: a review of progress made since 2011. *Metrologia* 51: R21–R30.

[126] Mise en Pratique (draft) for the kg in the New SI (2016) http://www.bipm.org/cc/CCM/Allowed/15/02A_MeP_kg_141022_v-9.0_clean.pdf (accessed on 10.01.2016).

[127] Mohr PJ, Taylor BN, Newell DB (2012) CODATA recommended values of the fundamental physical constants: 2010. *Rev. Mod. Phys.*, Vol. 84, No. 4.

[128] Mohr PJ, Phillips WD (2015) Dimensionless units in the SI. *Metrologia* 52:40–47.

[129] Mohr PJ, Phillips WD (2016) A proposal to classify the radian as a base unit in the SI. arXiv:1604.06774v1.

[130] Mohr PJ, Newell DB, and Taylor BN (2016) CODATA recommended values of the fundamental physical constants: 2014*. *Rev. Mod. Phys.*, 88(3): p. 035009

[131] Moldover MR et al (1988) Measurement of the Universal Gas Constant *R* Using a Spherical Acoustic Resonator, *Phys. Rev. Lett.* 60 249–52.

[132] Moldover MR, et al. (2014) Acoustic gas thermometry, *Metrologia*, 51(1), p. R1

[133] Molinar GF, Rebaglia B, Sacconi A, Legras JC, Vailleau GP, Schmidt, JW, Stoup JR, Flack DR, Sabuga W, Jusko O (1999) CCM key comparison in the pressure range 0.05 MPa to 1 MPa (gas medium, gauge mode): Phase A1: Dimensional measurements and calculation of effective area. *Metrologia* 36, 657 – 662.

[134] Neugebauer M, Lüdicke F, Bastam D, Bosse H, Reimann H, Töpperwien C (1997) A new comparator for measurement of diameter and form of cylinders, spheres and cubes under clean-room conditions. *Meas. Sci. Technol.* 8, 8, 849 – 856.

[135] Newell DB, Liard JO, Inglis AD, Eckl MC, Winester D, Silliker RJ and Gagnon CGL, The possible contribution of gravity measurements to the difference between the NIST and NRC watt balance results. *Metrologia* 50 (2013) 337–344.

[136] Nicolaus A (1993) Precise method to determining systematic errors in phase-shifting interferometry on Fizeau interferences. *Applied Optics,* 32, 31, 6380-86.

[137] Nicolaus A, Bönsch G (2005) Absolute volume determination of a silicon sphere with the spherical interferometer of PTB. *Metrologia*,42, 24–31.

[138] Nicolaus (2014) New Avogadro spheres for the redefinition of the kilogram. *Key Engineering Materials* 613, 17 – 25.

[139] Nyquist H (1928) Thermal agitation of electric charge in conductors. *Phys. Rev.*, 32, p. 110.

[140] Pearlman MR, Degnar JJ, Bosworth JM (2002) The International Laser Ranging Service. *Adv. Space Res.* 30: 135–143.

[141] Petley, BW (1987) Physical Constants and the SI, *NPL News* Jan. 1987.

[142] Picard A, Barat P, Borys M, Firlus M, Mizushima S (2011) State-of-the-art mass determination of ^{28}Si spheres for the Avogadro project. *Metrologia* 48: S112–S119.

[143] Pisani M et al. (2012) Comparison of the performance of the next generation of optical interferometers. *Metrologia* 49: 455–467.

[144] Planck M (1900) Über irreversible Strahlungsvorgänge. *Annalen der Physik*, 306 (1): 69–122.

[145] Planck M (1900) Zur Theorie des Gesetzes der Energieverteilung im Normalspektrum. *Verhandlungen der Dtsch. Phys. Ges.*, 2: p. 237.

[146] Plumb H, Cataland G (1966) Acoustical Thermometer and the National Bureau of Standards Provisional Temperature Scale 2–20 (1965). *Metrologia*, 2(4): p. 127.

[147] Pollinger F et al: (2015) Metrology for Long Distance Surveying: A Joint Attempt to Improve Traceability of Long Distance Measurements. *International Association of Geodesy Symposia*, Vol.143 pp 651-656.

[148] Pramann A, Rienitz O, Schiel D, Schlote J, Güttler B, Valkiers S (2011) Molar mass of silicon highly enriched in 28Si determined by IDMS. *Metrologia* 48 S20–S25.

[149] Pratt JR (2013) How to Weigh Everything from Atoms to Apples Using the Revised SI. *NCSLI Measure J. Meas. Sci.* Vol. 9 No. 1, 26 – 38.

[150] Preston-Thomas H (1990) The International Temperature Scale of 1990 (ITS-90). *Metrologia*, 27(1), p. 3.

[151] PTB workshop (2016) Round and ready - Dissemination of the kg via Si spheres.http://www.ptb.de/cms/presseaktuelles/messenevents/internationale-konferenzen/si-kg-2016/about-the-workshop.html (accessed 07.12.16).

[152] Puttock MJ, Thwaite EG (1969) Elastic compression of spheres and cylinders at point and line contact. *National Standards Laboratory* Technical Paper 25.

[153] Quincey P, Brown RJC (2016) Implications of adopting plane angle as a base quantity in the SI. *Metrologia* 53: 998 –1002.

[154] Quinn T (1989) News from the BIPM. *Metrologia*, 1989, 26(1), 69-74.

[155] Quinn T (2011) From artefacts to atoms: the BIPM and the search for ultimate measurement standards. *Oxford University Press*; 1 edition, ISBN: 978-0195307863.

[156] Quinn T, Quinn L, Davis R (2013) A simple watt balance for the absolute determination of mass, *Physics Education*, Volume 48, Number 5, 601.

[157] Richard P, Fang H, Davis R (2016) Foundation for the redefinition of the kilogram. *Metrologia* 53: A6–A11.

[158] Robinson I A and Kibble B P (2007) An initial measurement of Planck's constant using the NPL Mark II watt balance. *Metrologia* 44 427-40.

[159] Robinson I A (2012) Towards the redefinition of the kilogram: a measurement of the Planck constant using the NPL Mark II watt balance. *Metrologia* 49 113-156.

[160] Robinson IA (2016) Simplified fundamental force and mass measurements. *Metrologia* **53** 1054.

[161] Rosenband T et al. (2008) Frequency Ratio of Al+ and Hg+ Single-Ion Optical Clocks; Metrology at the 17th Decimal Place. *Science* 319 (5871): 1808–12.

[162] Sabuga W, Jusko O (1999) Effective area of the DHI Instruments piston-cylinder, piston P0107 and cylinder C012, calculated from the dimensional measurements data: phase A1 of the CCM comparison in gas media up to 1 MPa. *PTB-Bericht* PTB-ThEx-6, 21 p.

[163] Sanchez CA, Wood BM, Green RG, Liard JO and Inglis D (2014) A determination of Planck's constant using the NRC watt balance. *Metrologia* 51 S5–S14.

[164] Sanchez CA, Wood BM (2014) Alignment of the NRC watt balance: considerations, uncertainties and techniques. *Metrologia* 51 S42–S53.

[165] Saunders JB (1972) Ball and cylinder interferometer. *J. Res. Natl Bur. Stand.* 76C 11–20.

[166] Schlamminger S, Steiner RL, Haddad D, Newell DB, Seifert F, Chao LS, Liu R, Williams ER and Pratt JR (2015) A summary of the Planck constant measurements using a watt balance with a superconducting solenoid at NIST. *Metrologia* 52 L5–L8.

[167] Schmitt R et al. (2016) Advances in large-scale metrology - review and future trends. *CIRP Annals*: 65 2: 643 – 665.

[168] Scott, NE (1942) Egyptian Cubit Rods. *Metropolitan Museum of Art Bulletin*, New ser., v. 1, no. 1 (Summer, 1942) New York.

[169] Seifert F, Panna A, Li S, Han B, Chao L, Cao A, Haddad D, Choi H, Haley L and Schlamminger S (2014) Construction, Measurement, Shimming, and Performance of the NIST-4 Magnet System. *IEEE Trans. Instrum. Meas.*, 63(12).

[170] SI Brochure, Draft 9th edition (10 November 2016). (accessed 05.12.16) http://www.bipm.org/utils/common/pdf/si-brochure-draft-2016b.pdf

[171] Steiner R (2013) History and progress on accurate measurements of the Planck constant. *Rep. Prog. Phys.* 76, 016101 (46pp).

[172] Stenger J, Göbel EO (2012) The silicon route to a primary realization of the new kilogram. *Metrologia* 49 L25–L27.

[173] Stephenson AG, LaPiana LS, Mulville DR, Rutledge PJ, Bauer FH, Folta D, Dukeman, GA, Sackheim R, Norvig P (November 10, 1999) *Mars Climate Orbiter Mishap Investigation Board Phase I Report*, NASA. ftp://ftp.hq.nasa.gov/pub/pao/reports/1999/MCO_report.pdf (accessed 0412.16).

[174] Stock M et al. (2006) Final report on CCT-K7 key comparison of water triple point cell. *Metrologia*, 43(1A) p. 03001.

[175] Stock M, Barat P, Davis RS, Picard A and Milton MJT (2015) Calibration campaign against the international prototype of the kilogram in anticipation of the redefinition of the kilogram part I: comparison of the international prototype with its official copies. *Metrologia* 52 310–316.

[176] Sutton CM and Clarkson MT (2014) A magnet system for the MSL watt balance. *Metrologia* 51 S101–S106.

[177] Tanaka M et al. (2001) Recommended table for the density of water between 0 °C and 40 °C based on recent experimental reports. *Metrologia*, 38(4): p. 301.

[178] Tang Y, Ojha VN, Schlamminger S, Rüfenacht A, Burroughs CJ, Dresselhaus PD and Benz SP (2012) A 10 V programmable Josephson voltage standard and its applications for voltage metrology. *Metrologia* 49 635–643.

[179] Taylor B and Witt T (1989) New international electrical reference standards based on the Josephson and quantum Hall effects. *Metrologia*, vol. 26, no. 1, pp. 47–62.

[180] Taylor BN, Thompson A (Editors) (2008) The International System of Units (SI). *NIST Special Publication 330*, 2008 Edition.

[181] Thomas M, Espel P, Ziane D, Pinot P, Juncar P, Pereira Dos Santos F, Merlet S, Piquemal F and Genevès G (2015) First determination of the Planck constant using the LNE watt balance. *Metrologia* 52 433–443.

[182] Thomson W (Lord Kelvin) (1891) Lecture to the Institution of Civil Engineers on Electrical Units of Measurement, London (3 May 1883). *Popular Lectures and Addresses Vol. 1, 80-81* (London Macmillan and Co.).

[183] Underwood R et al. (2011) Dimensional characterization of a quasispherical resonator by microwave and coordinate measurement techniques. *Metrologia* 48(1): p. 1-15.

[184] Underwood R. et al. (2012) Pyknometric volume measurement of a quasispherical resonator. *Metrologia* 49(3): p. 245-256.

[185] Underwood R. et al. (2016) Estimates of the difference between thermodynamic temperature and the International Temperature Scale of 1990 in the range 118 K to 303 K. *Philosophical Transactions of the Royal Society A: Mathematical, Physical and Engineering Sciences*, 374 (2064).

[186] Vigoureux P (1965) A Determination of the Ampere. *Metrologia*, 1:3–7.

[187] v. Klitzing K, Dorda G and Pepper M, (1980) New Method for High-Accuracy Determination of the Fine-Structure Constant Based on Quantized Hall Resistance. *Phys. Rev. Lett.* 45, 494.

[188] Villar F, David J, and Genevès G (2011) 75 mm stroke flexure stage for the LNE watt balance experiment. *Precision Engineering* 35 693– 703.

[189] Weichert C et al. (2012) A heterodyne interferometer with periodic nonlinearities smaller than ±10 pm. *Meas. Sci. Technol.* 23: 094005 (7pp).

[190] White DR, Fischer J (2015) The Boltzmann constant and the new kelvin. *Metrologia* 52 S213.

[191] Zakel S, Wundrack S, Niemann H, Rienitz O, and Schiel D (2011) Infrared spectrometric measurement of impurities in highly enriched 'Si28'. *Metrologia* 48 S14–S19.

[192] Zhang JT, Lin H, Sun JP, Feng XJ, Gillis KA, Moldover MR (2010) Cylindrical Acoustic Resonator for the Redetermination of the Boltzmann Constant. *International Journal of Thermophysics - INT J THERMOPHYS*, vol. 31, no. 7, pp. 1273-1293.

[193] Zhang Z, He Q and Li Z (2006) An approach for improving the watt balance. *CPEM 2006 Conf. Digest* (Torino, Italy, July 2006) pp 126–7.

[194] Zhang Z, He Q, Li Z, Han B, Lu Y, Lan J, Li C, Li S, Xu J, Wang N, Wang G and Gong H (2014) The joule balance in NIM of China. *Metrologia* 51 S25–S31.

[195] Zosi G (1983) A neo-Pythagorean approach towards an atomic-mass standard. *Lett. Nuovo Cimento* 38 577–80.

[196] Zwinkels JC, Ikonen E, Fox NP, Ulm G and Rastello ML (2010) Photometry, radiometry and 'the candela': evolution in the classical and quantum world. *Metrologia*, Volume 47, Number 5, R15.